NACA RM A51F15

NACA

RESEARCH MEMORANDUM

SOME LOW-SPEED CHARACTERISTICS OF AN AIR-INDUCTION SYSTEM HAVING SCOOP-TYPE INLETS WITH PROVISIONS FOR BOUNDARY-LAYER CONTROL

By Earl C. Watson

Ames Aeronautical Laboratory
Moffett Field, Calif.

NATIONAL ADVISORY COMMITTEE
FOR AERONAUTICS

WASHINGTON

August 28, 1951

NATIONAL ADVISORY COMMITTEE FOR AERONAUTICS

RESEARCH MEMORANDUM

SOME LOW-SPEED CHARACTERISTICS OF AN AIR-INDUCTION SYSTEM HAVING SCOOP-TYPE INLETS WITH PROVISIONS FOR BOUNDARY-LAYER CONTROL

By Earl C. Watson

SUMMARY

An investigation was conducted at low speed of an air-induction system having twin scoop-type inlets on the sides of the fuselage of a model of an airplane designed for flight at supersonic Mach numbers. The leading edge of the lip of the scoop was rounded and there were provisions for control of the boundary layer ahead of the inlet.

An analysis of the data indicated that high external drag was associated with separation of the flow from the external surface of the lip. Several different profiles for the lip were investigated and one was chosen for further tests of the air-induction system. There was no separation from the external surface of the lip selected for mass-flow ratios above 0.75 at angles of attack between 1° and 11°, and at 0° angle of attack the ram-recovery ratio was the highest obtained.

For the lip profile chosen for detailed investigation operating with a ratio of boundary-layer-control duct flow to main duct flow of 0.075, data are presented showing the variation of the ram-recovery ratio in the main duct with mass-flow ratio, and the manner in which the ram-recovery ratio was affected by angle of attack and angle of sideslip. At 0° angle of attack and sideslip the ram-recovery ratio varied from 0.95 at a mass-flow ratio of 1.0 to 0.79 at a mass-flow ratio of 2.2. The ram-recovery ratio decreased about 0.05 with a change in angle of attack from 0° to 9°.

Some increase in the ram-recovery ratio in the main duct resulted from boundary-layer removal. For example, at a mass-flow ratio of 1.0, varying the boundary-layer-control duct flow from 0 to 0.075 of the main duct flow increased the ram-recovery ratio about 0.035.

Data are also presented which show the distribution of the ram-recovery ratio at the compressor inlet station, the pressure distributions on various surfaces, and the characteristics of the boundary layer in the vicinity of the entrance to the main scoop.

INTRODUCTION

There are limited data available on the low-speed characteristics of air-induction systems for use in airplanes designed for flight at supersonic speeds. The investigation reported in reference 1 was concerned with the low-speed characteristics of a fuselage side inlet for use at transonic flight speeds; that reported in reference 2 was concerned with the low-speed characteristics of two supersonic inlets having sharp leading edges, one designed for flight Mach numbers up to 1.2, and the other for flight Mach numbers up to 3.0. In each of these investigations the inlets were annular with a conical central body. The investigation of reference 3 was made to determine the subsonic characteristics of air-induction systems for a hypothetical airplane which would utilize scoop-type inlets designed for a Mach number of 1.7. These investigations indicated that separation of the flow from the internal surfaces of the lips occurred at high mass-flow ratios and reduced the pressure recoveries of the inlets, and that separation of the flow from the external surfaces of the lips occurred at low mass-flow ratios and increased the external drag.

As part of a program for the development of a supersonic research airplane, an experimental investigation was undertaken of an air-induction system which had twin scoop-type inlets on the sides of the fuselage. The forebody of the fuselage, which was approximately triangular in cross section, was designed to produce external supersonic compression of the air by utilizing the conical shock wave at the nose and an oblique shock wave at each intake ramp. A rounded lip was employed and thus a normal shock wave and a region of subsonic air flow would always occur just ahead of each main scoop. A boundary-layer scoop was located at the leading edge of each intake ramp in order to reduce the quantity of low-energy air entering the main ducts and to reduce the boundary-layer and shock-wave interaction at supersonic speeds.

The results of tests of a simplified version of the design at supersonic speeds are given in reference 4. The results of tests of a 1/4-scale model of the design at low subsonic speeds are presented herein. This investigation, made for various angles of attack, angles of sideslip, and mass-flow ratios in the main and boundary-layer-control ducts, was concerned with the following:

1. The flow conditions over the lips of the main scoops and the development, if necessary, of a lip profile over which there would be no separation of the flow from the external surface for mass-flow ratios between 0.75 and 1.0 (the range of mass-flow ratio expected for the operation of these inlets at subsonic speeds);

2. The pressure-recovery characteristics of the main and boundary-layer-control ducts;

3. The pressure distributions on various surfaces; and

4. The characteristics of the boundary layer in the vicinity of the entrance to the scoops.

NOTATION

Symbols

A	duct cross-sectional area, square feet
a	speed of sound in air, feet per second
C_{D_S}	wake-survey drag coefficient based on the entrance area of the main duct
D	drag, pounds
h	distance normal to a surface, inches
H	total pressure, pounds per square foot
M	Mach number $\left(\frac{V}{a}\right)$
p	static pressure, pounds per square foot
P	pressure coefficient $\left(\frac{p_l - p_o}{q_o}\right)$
q	dynamic pressure, pounds per square foot
u	local velocity in the boundary layer, feet per second
U	local velocity immediately outside of the boundary layer, feet per second

V velocity, feet per second

α geometric angle of attack of the fuselage reference plane, degrees
(Nose up is the positive direction.)

β angle of sideslip, the angle between the fuselage plane of symmetry and the flight path, degrees
(Nose to the left is the positive direction.)

δ thickness of the boundary layer to where the local velocity u is 0.99 of the velocity U outside the boundary layer

δ^* boundary-layer displacement thickness $\left[\int_0^{\delta}\left(1-\frac{u}{U}\right)dh\right]$

θ boundary-layer momentum thickness $\left[\int_0^{\delta}\frac{u}{U}\left(1-\frac{u}{U}\right)dh\right]$

φ angular position of the pressure tubes in the rake at the station corresponding to the compressor inlet, measured clockwise about the center of the main duct from the duct vertical reference line as viewed looking forward

ρ mass density of the air, slugs per cubic foot

$1+\eta$ compressibility factor $\left(1+\frac{1}{4}M^2+\frac{1}{40}M^4+\frac{1}{1600}M^6\ldots\right)$

Subscripts

o free stream

1 station at which the entrance area of the main duct was determined, station 294

2 simulated compressor inlet, station 394.5

B boundary-layer-control duct

l local position

Parameters

$\frac{H - p_o}{H_o - p_o}$ ram-recovery ratio

$\frac{m_1}{m_o}$ mass-flow ratio in the main duct $\left(\frac{\rho_1 A_1 V_1}{\rho_o A_1 V_o}\right)$

$\frac{m_B}{m_1}$ ratio of the mass flow through the boundary-layer-control duct to the mass flow through the main duct $\left(\frac{\rho_B A_B V_B}{\rho_1 A_1 V_1}\right)$

DESCRIPTION OF MODEL AND APPARATUS

The model was one-fourth full size and was mounted on its left side as shown in figure 1. A more detailed view showing the scoops on the right side of the model can be seen in figure 2. Station numbers on the fuselage and dimensions, unless otherwise indicated, are in inches, full scale.

After some preliminary testing the model was revised to conform with proposed changes to the fuselage and air-induction systems of the airplane. From these tests it was found that closing the ducts on one side of the model at the plenum chamber did not affect the characteristics of the ducts on the other side. Thus, only the right side of the model was revised to the appropriate contours and the ducts on the left side were sealed at the plenum chambers. Some of the changes can be seen in figure 1 by comparing the right and left sides of the model. It should be noted that the data presented in this report are only for the revised right side of the model.

A portion of the revised main scoop between stations 291 and 300 was so designed that it could be removed in order that different profiles for the lip of the scoop could be investigated. The details of the orientation of the lip are shown in figure 3, together with the pertinent dimensions and contours of the fuselage and the scoops. The profiles of the lips investigated are shown in figure 4 and the coordinates are given in table I. The internal profiles of all the lips faired to the duct contour at station 300. Lip E and lip O had the same internal profile. The external profile of lips O, B, D, and F was designed to fair to the contour of the scoop surface at station 300. For lips E and G the external profile was faired to the scoop surface at station 325.

Figure 5 shows the longitudinal variation of the area of the main duct. The ratio of the area at station 394.5, the station corresponding

to the entrance to the compressor of the engine, to the entrance area of the main duct was 1.267. The entrance area, which was defined as that at station 294, was 248 square inches.

The starter housing with the spinner, and the starter-housing struts, which had the NACA 0024 airfoil section with a full-scale chord of 3.125 inches, are shown in figure 2.

Pressure recovery in the main duct was calculated from measurements at station 394.5. The rake used to obtain the measurements can be seen in figure 2. The orientation of the 76 total-pressure tubes and the 8 static-pressure tubes of the rake is shown in figure 6.

The pressure recovery in the boundary-layer-control duct was calculated from measurements at station 291, and the orientation of the pressure tubes is shown in figure 6.

Other instrumentation of the model included flush orifices along the canopy, along the intake ramp, and along the top and floor of the duct in the plane through the center of the duct. The flush orifices in the scoop surface forward of station 300 were in the same plane, but behind station 300 they were in the plane designated Z_D in figure 3.

Removable rakes were used to measure pressures in the wake from the lip of the main scoop and in the boundary layer ahead of the main scoop.

The 76 total-pressure tubes of the rake in the main duct were connected to an integrating water-in-glass manometer which provided the individual as well as the arithmetic mean of the total pressures. Because of the spacing of the tubes this arithmetic mean was approximately the same as the area-weighted-average ram-recovery ratio. All other pressure tubes were connected to multiple manometers. Readings of all manometers were recorded photographically.

A plenum chamber for the main ducts and a plenum chamber for the boundary-layer-control ducts were inside the model, and an individual piping system connected each chamber with a separate blower.

The quantity of air flow through the main ducts was regulated by means of a centrifugal blower driven by an electric motor, and was metered by means of a calibrated A.S.M.E. orifice meter in the piping system. The quantity of air flow through the boundary-layer-control ducts was regulated and metered in a similar manner.

Tests

The tests were conducted in one of the Ames 7- by 10- foot wind tunnels at a Reynolds number of approximately 1.4×10^6 for a length of 1 foot. The free-stream Mach number was approximately 0.16.

Static pressures on the external and internal surfaces of the lip, and static and total pressures in the wake of the lip and at the compressor inlet station were measured for each of the lips tested. The data from these measurements, together with tuft observations, provided a basis for comparing the lips. The profile of lip E was selected and used for further tests. Unless otherwise specified, the data presented in this report are for lip E on the right main scoop. With this lip, tests were made for the following range of variables:

1. Main duct mass-flow ratio (m_1/m_0) . . . . . 0 to 4.0

2. Ratio of the mass flow through the boundary-layer-control duct to the mass flow through the main duct, m_B/m_1 . . . . . 0 to 0.15

3. Angle of attack, α . . . . . 0° to $+21^\circ$

4. Angle of sideslip, β . . . . . 0°, -10°, and $+10^\circ$

The ratio of the mass flow through the boundary-layer-control duct to the mass flow through the main duct m_B/m_1 was 0.075, except when the primary concern was to measure boundary-layer velocity profiles or to investigate the flow in the boundary-layer-control duct. Zero flow in the boundary-layer-control duct was obtained in two ways: In one the boundary-layer-control duct was sealed at the plenum chamber, and in the other a plasticene fairing was used from the intake ramp to the canopy.

RESULTS AND DISCUSSION

Characteristics of the Lips Investigated

A region of separated flow over the external surface of the original lip, lip 0, of the main scoop was indicated during the tests of the model. The profile of the lip was modified in an attempt to (1) eliminate separation from its external surface for mass-flow ratios above 0.75 (a mass-flow ratio of 0.75 was chosen as the lowest mass-flow ratio that might be encountered with the airplane at subsonic speeds), and (2) to improve the pressure recovery at the compressor-inlet station.

Pressure distributions on the external surfaces of the lips are presented in figures 7(a) through 7(f) for a model angle of attack of 0°. Separation of the flow from the external surface of lip 0, the original lip, occurred as the mass-flow ratio was reduced from 1.0 to 0.8. This separation is indicated in figure 7(a) by the collapse of the region of minimum pressure near the leading edge of the lip into an extended region of less negative pressure. As the mass-flow ratio was further reduced to 0.6, the region of relatively constant pressure was enlarged and the minimum pressure coefficient became less negative. The pressure coefficients shown in figure 7 are an indication of the flow conditions over the lip and scoop surface near the plane Z_D only. Tuft studies were made to determine the lowest mass-flow ratio for unseparated flow as a function of the angle of attack. Figure 8 shows the lowest mass-flow ratio for unseparated flow over the external surfaces of lips 0, E, and F for angles of attack between 0° and 15°. The tuft studies indicated that the separation originated at the leading edge of the lips. At low angles of attack it occurred first from the lower surface of the scoop; at high angles of attack it occurred first from the upper surface. (See fig. 3, view C-C for surface designations.) Data for 0° angle of attack indicated that the flow over lip B was attached for mass-flow ratios down to 0.6, and that over lips D and G the flow was attached at a mass-flow ratio of 0.4. Tuft studies were not made throughout the range of angle of attack with lips B, D, and G. The data for 0° angle of attack indicated that these lips would be satisfactory from the standpoint of external separation; however, the ram-recovery ratio in the main duct was adversely affected by these lips at high mass-flow ratios, as is evident from figure 9.

Figure 9 shows the variation of ram-recovery ratio with mass-flow ratio in the main duct for the six lips. The lowest ram-recovery ratios were obtained with the most drooped lips (lips B, D, and G, see fig. 4). Large differences in the ram-recovery ratios for the lips occurred only at high mass-flow ratios, above 1.6, such as those which may be encountered during take-off. These differences were attributed to the relative degree of separation of the flow from the internal surfaces of the lips. It can be seen in figure 9 that the ram-recovery ratio in the main duct was highest with lip E.

For further investigation of the air-induction system the profile of lip E, which was thicker and of different camber than the original lip, was selected for the scoop. Lip E was chosen because there was no separation of the flow from the external surface for mass-flow ratios above 0.75, for angles of attack between 1° and 11°, and at 0° angle of attack the ram-recovery ratio in the main duct was the highest obtained.

To estimate the effect of separation of the flow on the drag of the lip, pressure measurements were obtained in the wake of lips 0 and E at station 357. These measurements were made at three different positions on the surface of the scoop. (See fig. 2.) Evaluation of the pressures

by the method suggested in reference 5 gave a relative subsonic drag coefficient for each lip. The wake-survey drag coefficients, based upon the entrance area, are shown for each of these two lips in figure 10 for a range of mass-flow ratio and angle of attack. The drag coefficients for each lip were about the same when there was no separation from either lip, that is, the values of the wake-survey drag coefficient for lip O at a mass-flow ratio of 1.2 were about the same as the values for lip E at a mass-flow ratio of 0.8. For equal mass-flow ratios between 0.60 and 1.0 the drag of lip E was considerably less than that of lip O. It is evident that separation from an improperly designed lip, such as lip O, would have a considerable effect on the drag of the fuselage.

Characteristics of the Main Duct With Lip E

The pressure recovery in the main duct varied with the mass-flow ratio of the main duct, with the angle of attack, with the angle of sideslip, and with the quantity of air flow in the boundary-layer-control duct. Figure 11 shows the variation of the ram-recovery ratio at the compressor inlet station with the mass-flow ratio for the main duct with lip E. The ram-recovery ratio computed on the basis of isentropic flow and a duct efficiency $\left(\frac{H_2-p_1}{H_1-p_1}\right)$ of 0.97 also is shown in figure 11. Because the difference between the two curves was nearly constant for mass-flow ratios between 1.0 and 2.2, it can be assumed that there was no separation of the flow from the internal surface of the lip. For increasing mass-flow ratios above 2.2 the difference between the two curves increased rapidly and thereby indicated a decrease in ram-recovery ratio probably resulting from separation of the flow.

For power-on static conditions, which would be encountered prior to take-off, the mass-flow ratio of the duct becomes infinite. For this condition, the pressure-loss coefficient is presented in figure 12 as a function of the impact pressure at the entrance of the duct. The impact pressure was calculated assuming isentropic flow from free stream to the inlet, and at its highest value the Mach number at the entrance of the duct was approximately 0.34.

Figure 13 shows the variation of ram-recovery ratio in the main duct with angle of attack for constant mass-flow ratios. Changing the angle of attack from 0° to 9° reduced the ram-recovery ratio about 0.05, or less, depending on the mass-flow ratio. The rate of change of ram-recovery ratio with angle of attack was greater at angles above 9°. The combined effects of changes of angle of attack and mass-flow ratio on the ram-recovery ratio are shown in a three-dimensional plot in

figure 14, which shows conveniently the adverse effects of high mass-flow ratio and angle of attack.

Figures 15(a) through 15(f) show the effects of angle of sideslip on the ram-recovery ratio in the main duct for various angles of attack and mass-flow ratios.

The circumferential distributions of the ram-recovery ratio at three different radial distances from the duct wall at the compressor inlet station are shown in figure 16(a) through 16(f) for various mass-flow ratios and an angle of attack of 0°. At the radial distance closest to the duct wall the circumferential variations in the ram-recovery ratio were greater than at the other two radial distances by an amount which varied with the mass-flow ratio. The greatest variation – indicative also of the largest pressure losses – occurred in the region which would be most influenced by the flow along the floor and from the corners of the duct. Exploratory pressure surveys indicated that large pressure losses originated in the corners at the entrance of the duct presumably because of local flow separation.

Figures 17(a) and 17(b) show that the maximum measured circumferential variation of the ram-recovery ratio was from about 0.15 to 1.7 for mass-flow ratios between 0.5 and 2.4, respectively. Parts (a) and (b) show the effects of angle of attack and of angle of sideslip, respectively. Also shown in this figure is the computed circumferential variation of ram-recovery ratio based upon a circumferential variation of total pressure at the compressor inlet of 1 pound per square inch for standard sea level conditions. Note that below a mass-flow ratio of about 1.2 the measured variation exceeded the computed variation. Whether such a circumferential variation of total pressure is excessive or not would depend upon its effect on the engine.

Characteristics of the Boundary-Layer-Control Duct

The influence of the variation of the quantity of flow in the boundary-layer-control duct on the pressure recovery in the main duct can be seen in figure 18. The data for the value of $m_B/m_1 = 0$ were obtained with the boundary-layer-control duct sealed at the plenum chamber. As can be seen in the figure, the largest portion of the gain in ram-recovery ratio which resulted from a variation of m_B/m_1 from 0 to 0.15 was realized when m_B/m_1 was 0.075.

At a mass-flow ratio of 1.0, varying m_B/m_1 from 0 to 0.075 increased the ram-recovery ratio approximately 0.035. When a plasticene fairing from the intake ramp to the canopy was used to seal the boundary-layer-control duct, the increase was approximately 0.025.

Thus, at subsonic speeds it may not be necessary to remove the boundary layer for this type of inlet combination particularly if there is proper fairing between the intake ramp and the canopy.

Figure 19 shows the variation of the ram-recovery ratio in the boundary-layer-control duct with the quantity-of-flow parameter m_B/m_1 for various mass-flow ratios in the main duct. Figure 20 shows this variation in a three-dimensional plot which conveniently indicates that the pressure recovery in the boundary-layer-control duct was adversely affected by a combination of high mass-flow ratio in the main duct and a high value of the ratio of boundary-layer-control-duct flow to main-duct flow.

The effects of angle of attack and angle of sideslip on the ram-recovery ratio in the boundary-layer-control duct are shown in figures 21 and 22, respectively, for $m_B/m_1 = 0.075$. The low pressure recovery in the boundary-layer-control duct throughout the range of variables of the test can be attributed mainly to the low energy of the air in the boundary layer.

Pressure Coefficient Distributions and Boundary-Layer Characteristics

Pressure coefficient distributions on the canopy, on the intake ramp, on the top and floor of the main duct, and on the scoop surface are presented in figure 23 for various mass-flow ratios and in figure 24 for various angles of attack. At a mass-flow ratio of 1.6 the pressure coefficients on the top and floor of the duct were only affected slightly by angles of attack up to 15°.

Figure 25 shows the momentum and displacement thicknesses of the boundary layer ahead of the main scoop for a wide range of flow conditions in both the main and boundary-layer-control ducts. For mass-flow ratios between 0.6 and 1.6, the pressure distributions and boundary-layer profiles for the canopy and intake ramp indicated that there was no separation of the flow ahead of the main scoop for any of the quantities of flow in the boundary-layer-control duct.

CONCLUDING REMARKS

A wind-tunnel investigation at low speed was made of the air-induction system of a model of an airplane fuselage designed for flight at supersonic Mach numbers. The data presented are an indication of the conditions of the flow over the surface of the scoop, over the intake

ramp, over the canopy, and of the flow in the main and boundary-layer-control ducts. The more important results and conclusions which were reached are as follows:

1. Data and observations from this investigation indicated that the profile of the original lip for the main scoop would be unsatisfactory for subsonic speeds because the flow over the external surface of the lip was separated for mass-flow ratios of 1.0 and less. Several different profiles for the lip of the scoop were investigated and of these one was selected for further tests of the air-induction system. This improved lip was thicker and of different camber than the original lip. With this lip on the main scoop, the flow over the external surface was unseparated at angles of attack between 1° and 11° for mass-flow ratios of 0.75 and above, and at 0° angle of attack the pressure recovery in the main duct was improved at high mass-flow ratios.

2. For a given angle of attack and for a given mass-flow ratio below 1.0, the drag of the main scoop, as indicated by the wake-survey drag coefficient, was much larger with the original lip than with the improved lip.

3. At 0° angle of attack and with the improved lip, the ram-recovery ratio in the main duct varied from 0.95 at a mass-flow ratio of 1.0 to 0.79 at a mass-flow ratio of 2.2 for a ratio of boundary-layer-control-duct flow to main-duct flow of 0.075. Increasing the angle of attack up to 9° gradually decreased the ram-recovery ratio (a decrease of about 0.05 or less). Above 9° the ram-recovery ratio decreased more rapidly.

4. Some increase in ram-recovery ratio in the main duct resulted from boundary-layer removal. At a mass-flow ratio of 1.0, varying the quantity of flow in the boundary-layer-control duct from 0 to 0.075 of the flow in the main duct increased the ram-recovery ratio approximately 0.035.

Ames Aeronautical Laboratory,
National Advisory Committee for Aeronautics,
Moffett Field, California.

REFERENCES

1. Nichols, Mark R., and Goral, Edwin B.: A Low-Speed Investigation of a Fuselage-Side Air Inlet for Use at Transonic Flight Speeds. NACA RM L7A06, 1947.

2. Dennard, John S.: An Investigation of the Low-Speed Characteristics of Two Sharp-Edge Supersonic Inlets Designed for Essentially External Supersonic Compression. NACA RM L7D03, 1947.

3. Holzhauser, Curt A.: An Experimental Investigation at Subsonic Speeds of a Scoop-Type Air-Induction System for a Supersonic Airplane. NACA RM A51E24, 1951.

4. Edwards, Sherman S.: Experimental Investigation at Supersonic Speeds of Side Scoops Employing Boundary-Layer Suction. NACA RM A9I29, 1949.

5. Baals, Donald D., and Mourhess, Mary J.: Numerical Evaluation of the Wake-Survey Equations for Subsonic Flow Including the Effect of Energy Addition. NACA ARR L5H27, 1945. Nov. 1945.

TABLE I.- THE COORDINATES OF THE LIPS
[Dimensions are in inches, full scale]

	Lip O		Lip B		Lip D		Lip E		Lip F		Lip G	
x \ y	Internal	External	Internal	External	Internal	External	Internal	External	Internal	External	Internal	External
0.000	0	0	-0.500	-0.500	-1.125	-1.125	0	0	-0.150	-0.150	-0.200	-0.200
.005	- - -	.030	- - -	- - -	- - -	- - -	- - -	- - -	- - -	- - -	- - -	- - -
.015	- - -	.050	- - -	- - -	- - -	- - -	- - -	- - -	- - -	- - -	- - -	- - -
.020	-.090	- - -	-.570	-.360	- - -	- - -	-.090	.100	-.210	-.065	-.305	-.100
.035	- - -	.065	- - -	- - -	- - -	- - -	- - -	- - -	- - -	- - -	- - -	- - -
.050	-.145	- - -	-.610	-.330	-1.235	-.900	-.145	.170	-.265	-.010	-.345	-.045
.066	- - -	.095	- - -	- - -	- - -	- - -	- - -	- - -	- - -	- - -	- - -	- - -
.100	-.200	.115	-.655	-.270	-1.285	-.815	-.200	.235	-.325	.045	-.405	.025
.125	- - -	- - -	- - -	- - -	- - -	- - -	- - -	.265	- - -	- - -	- - -	- - -
.190	- - -	- - -	- - -	- - -	- - -	- - -	- - -	.320	- - -	- - -	- - -	- - -
.200	-.285	- - -	-.720	-.195	-1.365	-.690	-.285	- - -	-.395	.125	-.475	.140
.250	- - -	.170	- - -	- - -	- - -	- - -	- - -	- - -	- - -	- - -	- - -	- - -
.300	-.345	- - -	-.790	-.125	-1.410	-.605	-.345	- - -	-.450	.175	-.520	.230
.320	- - -	- - -	- - -	- - -	- - -	- - -	- - -	.410	- - -	- - -	- - -	- - -
.400	- - -	- - -	-.825	-.070	-1.450	-.530	- - -	- - -	- - -	- - -	- - -	- - -
.500	-.435	.220	-.860	-.025	-1.470	-.470	-.435	- - -	-.530	.250	-.580	.365
.640	- - -	- - -	- - -	- - -	- - -	- - -	- - -	.565	- - -	- - -	- - -	- - -
.700	-.505	- - -	-.900	.050	-1.505	-.350	-.505	- - -	-.590	.310	-.625	.480
.900	-.560	- - -	-.925	.125	-1.525	-.255	-.560	.650	- - -	- - -	- - -	- - -
1.000	- - -	.290	- - -	- - -	- - -	- - -	- - -	- - -	-.645	.375	-.670	.595
1.200	-.625	- - -	-.935	.220	-1.540	-.110	-.625	- - -	- - -	- - -	- - -	- - -
1.500	-.670	- - -	-.930	.305	-1.540	.015	-.670	.755	-.710	.465	-.725	.735
1.900	-.715	- - -	- - -	- - -	- - -	- - -	-.715	- - -	- - -	- - -	- - -	- - -
2.000	- - -	.435	-.925	.420	-1.530	.205	- - -	.820	-.740	.520	-.740	.820
2.300	-.740	- - -	-.920	.475	-1.515	.315	-.740	- - -	- - -	- - -	- - -	- - -
2.700	-.750	- - -	- - -	- - -	- - -	- - -	-.750	- - -	- - -	- - -	- - -	- - -
3.000	- - -	.565	-.910	.565	-1.430	.525	- - -	.915	-.750	.635	-.750	.915
4.000	- - -	- - -	- - -	- - -	- - -	- - -	- - -	- - -	-.745	.730	-.745	.990
5.000	-.750	.830	- - -	- - -	- - -	- - -	- - -	1.075	- - -	- - -	- - -	- - -
9.000	-.600	1.190	-.600	1.190	-.600	1.190	-.600	1.345	-.600	1.190	-.600	1.345

NACA

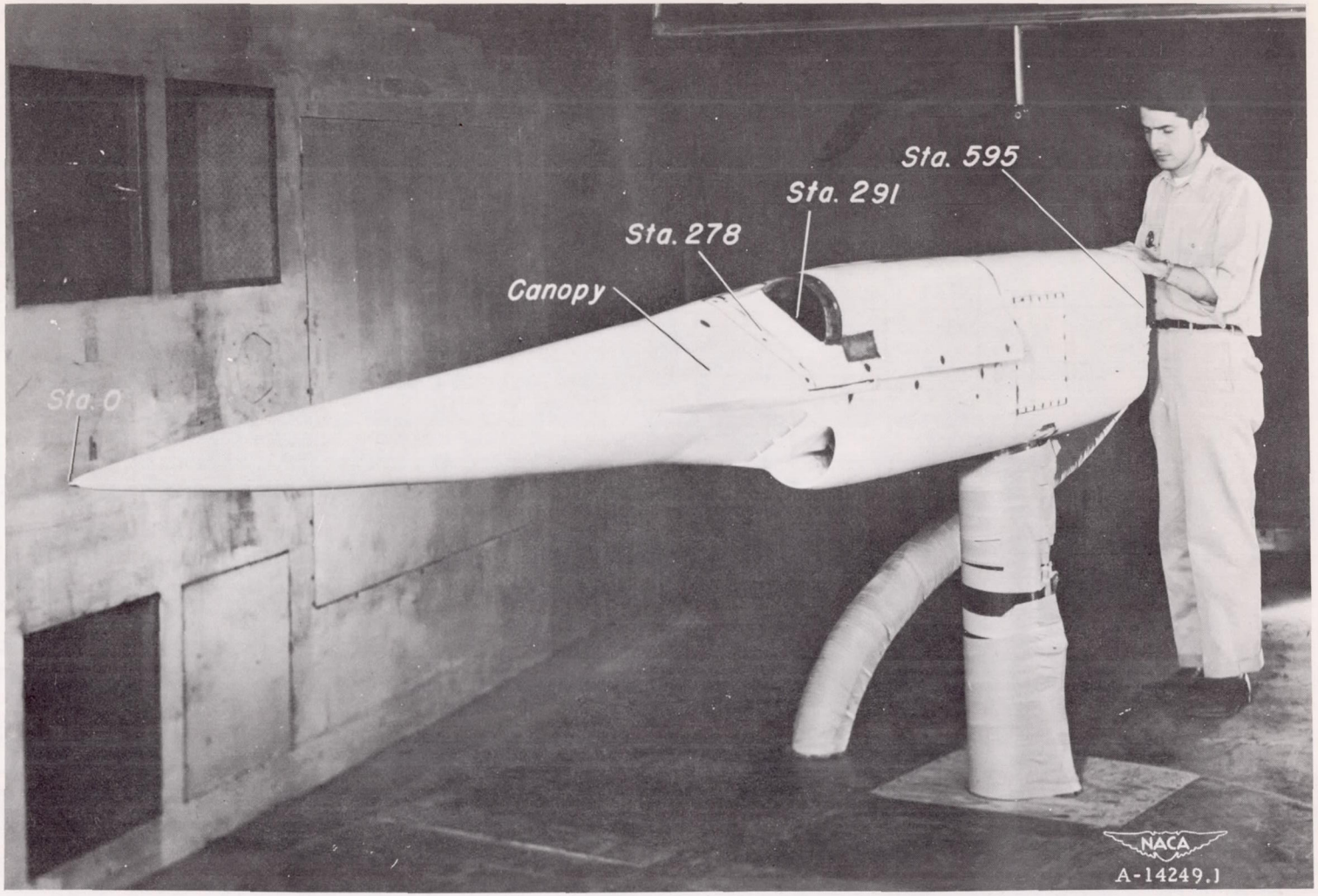

Figure 1.– The model mounted in one of the Ames 7– by 10–foot wind tunnels.

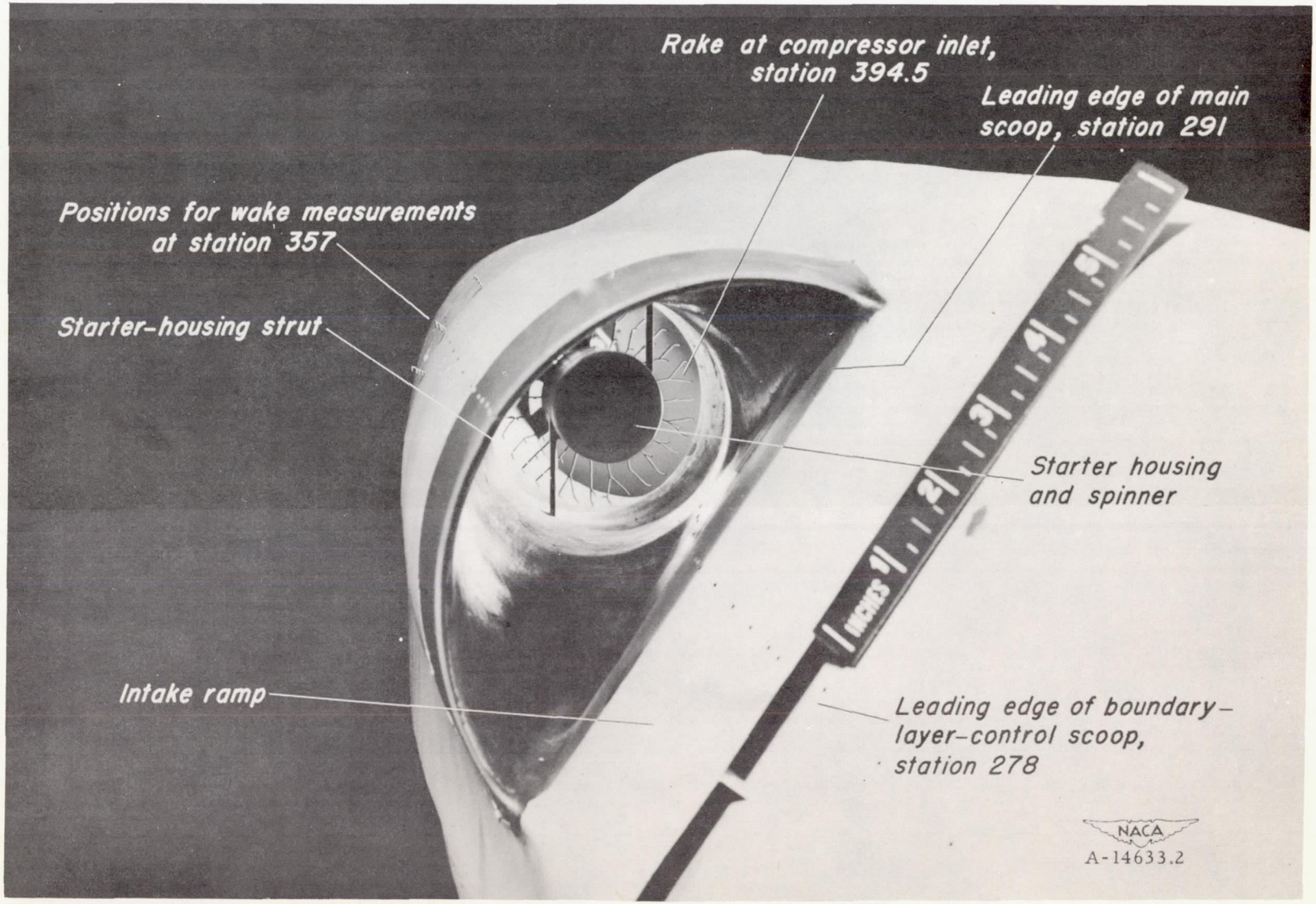

Figure 2.- The main scoop on the right side of the model.

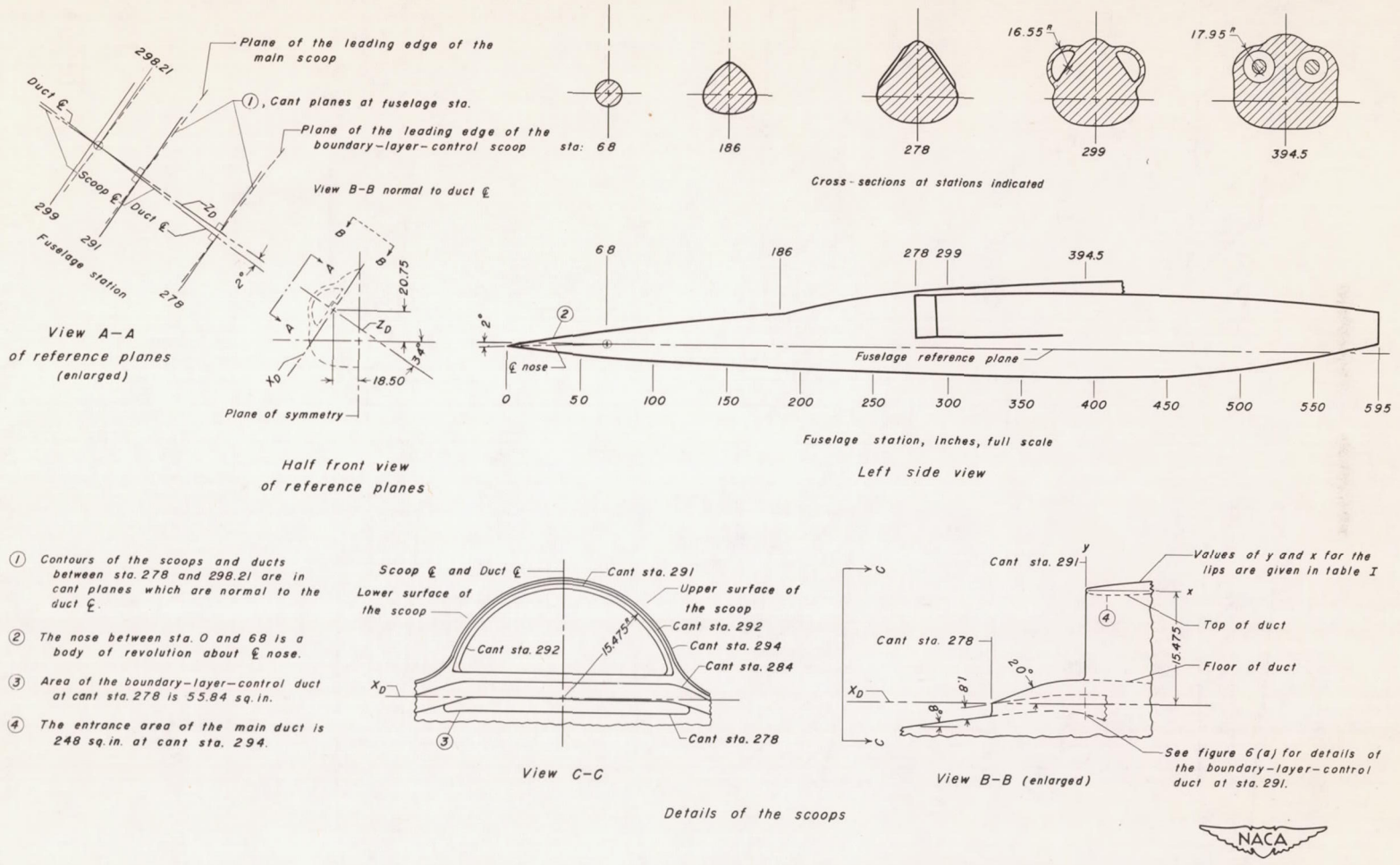

Figure 3.—The orientation of the fuselage and the scoops.

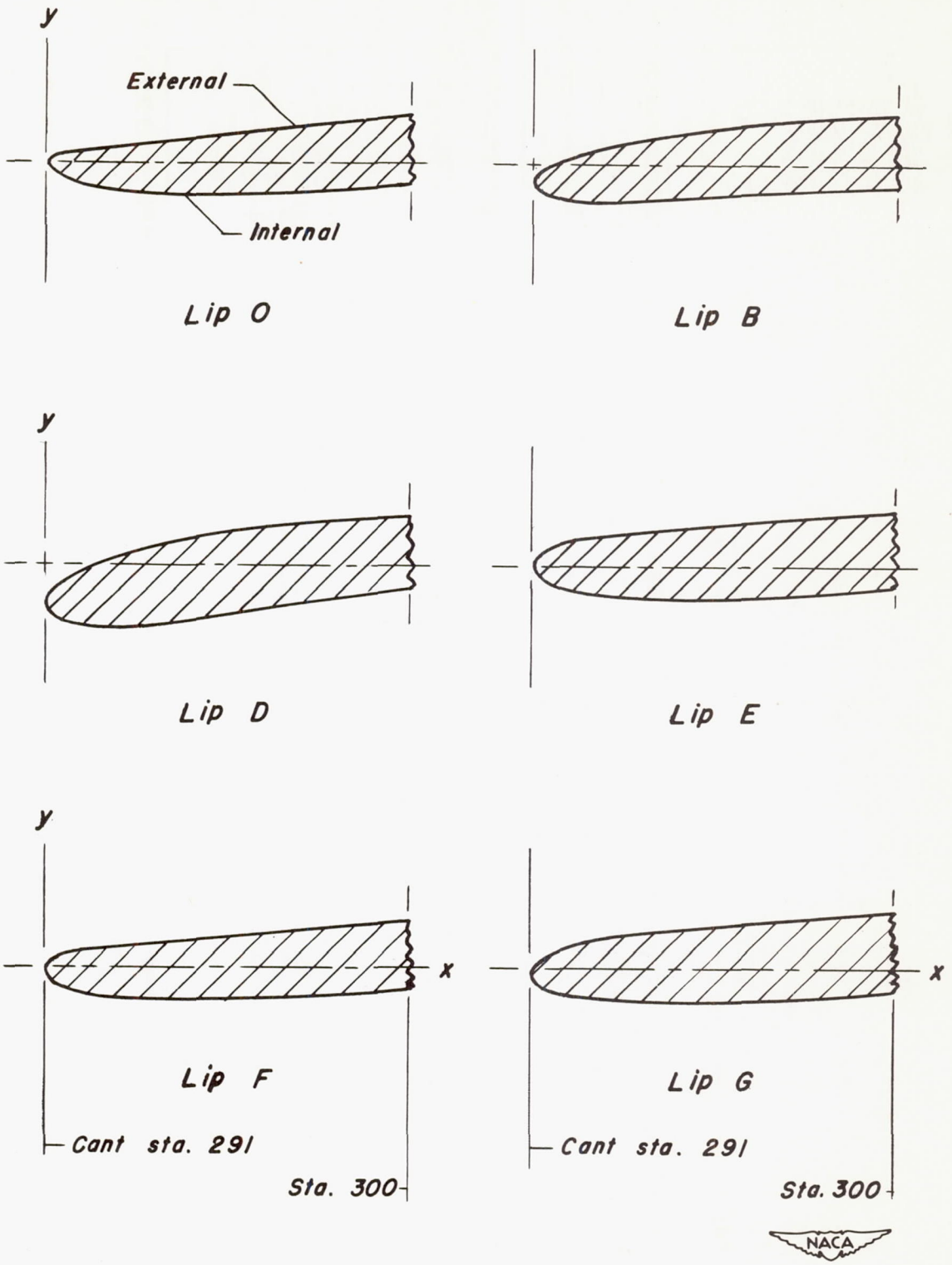

Figure 4.- The profiles of the lips.

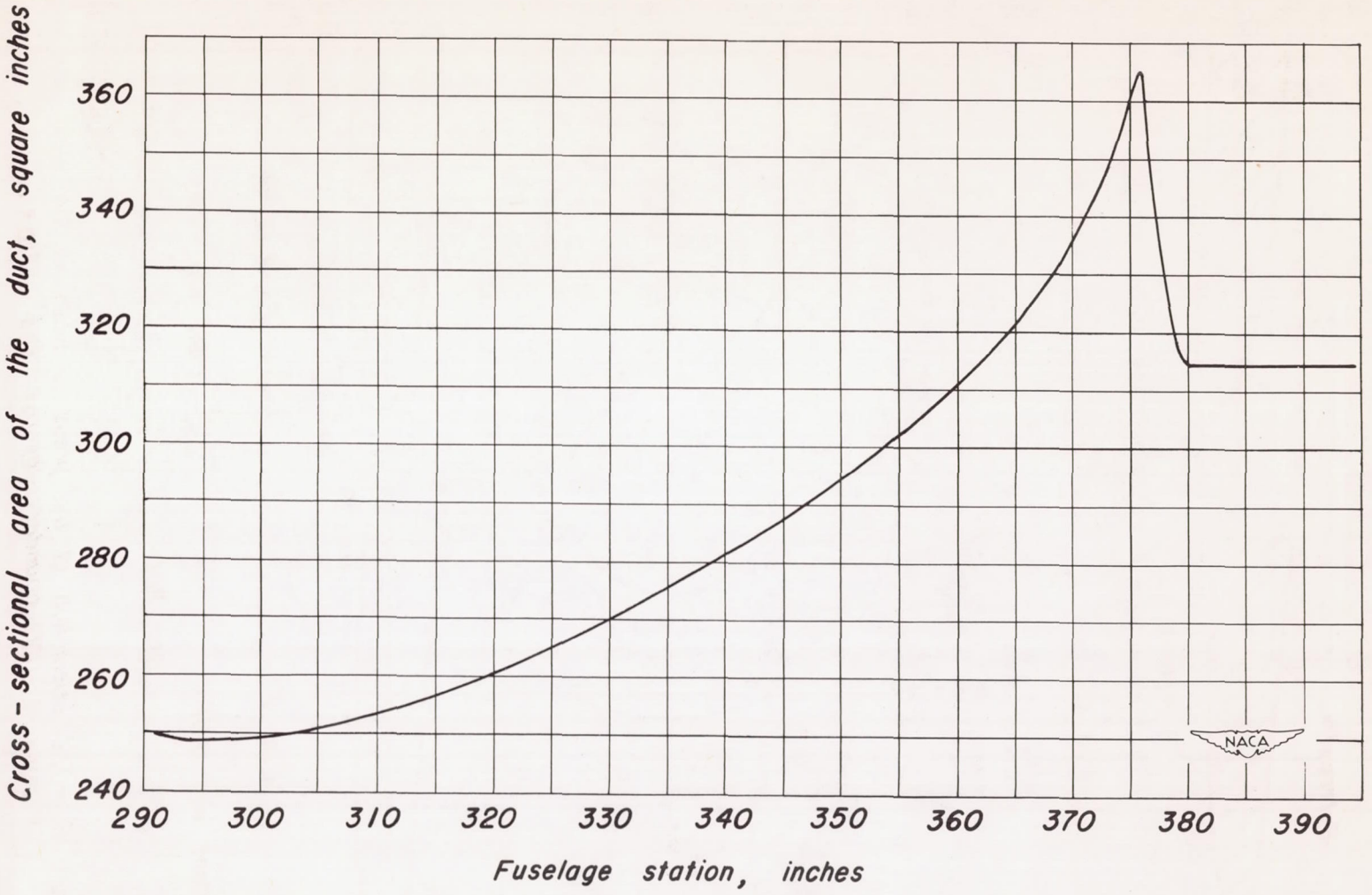

Figure 5 .- The variation of the cross-sectional area of the main duct with fuselage station.

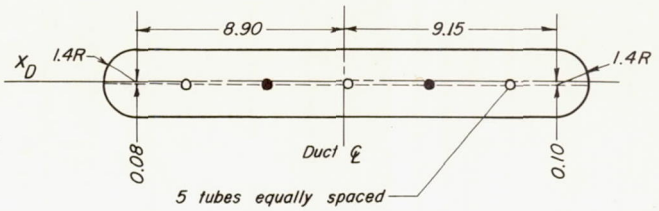

(a) Pressure tubes in the boundary-layer-control duct at cant station 291.

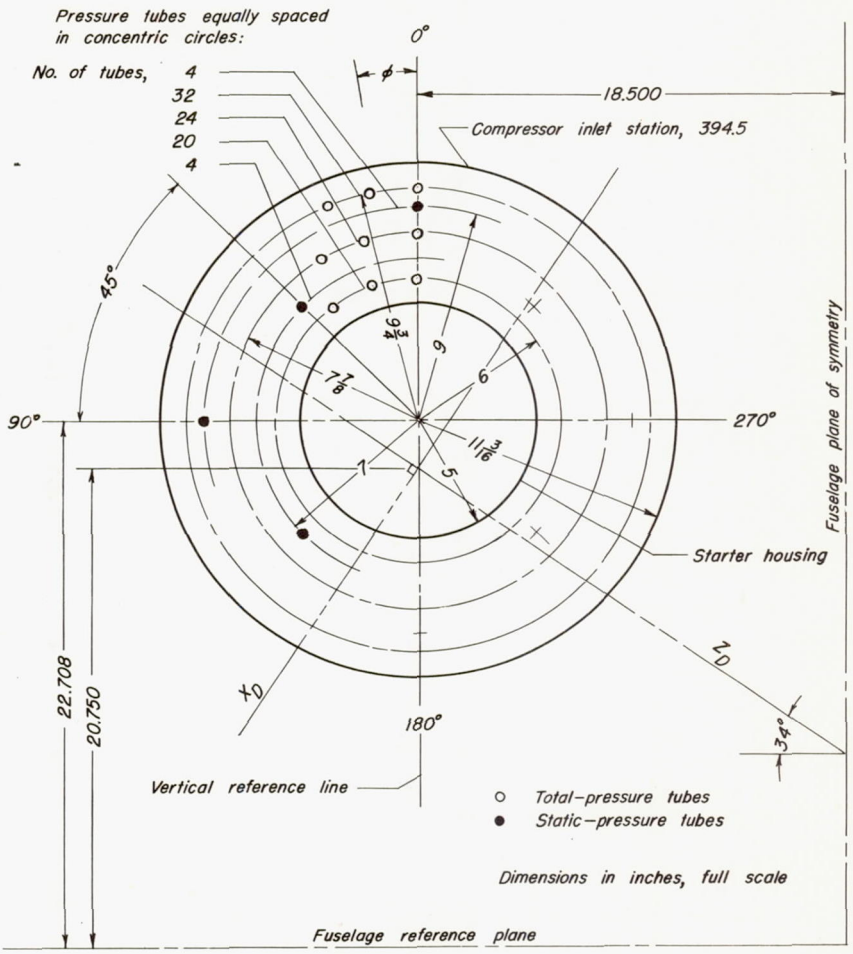

(b) Pressure tubes in the main duct at the compressor inlet station.

NACA

Figure 6.—The orientation of the pressure tubes in the main and in the boundary-layer-control ducts.

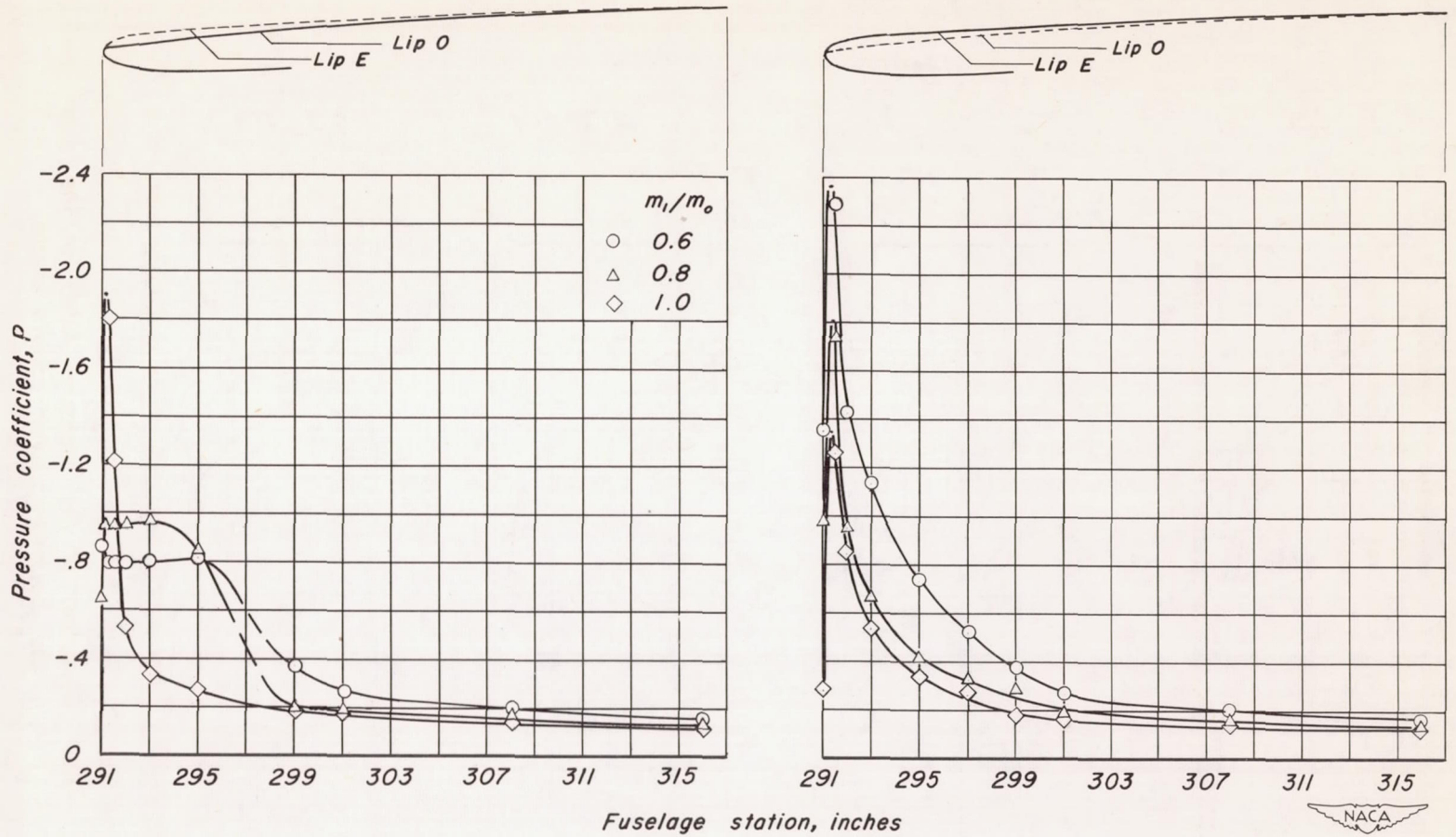

(a) Lip O.

(b) Lip E

Figure 7.– The pressure coefficients for the external surfaces of the lips. $\alpha = 0°$; $\beta = 0°$; $m_B/m_1 = 0.075$.

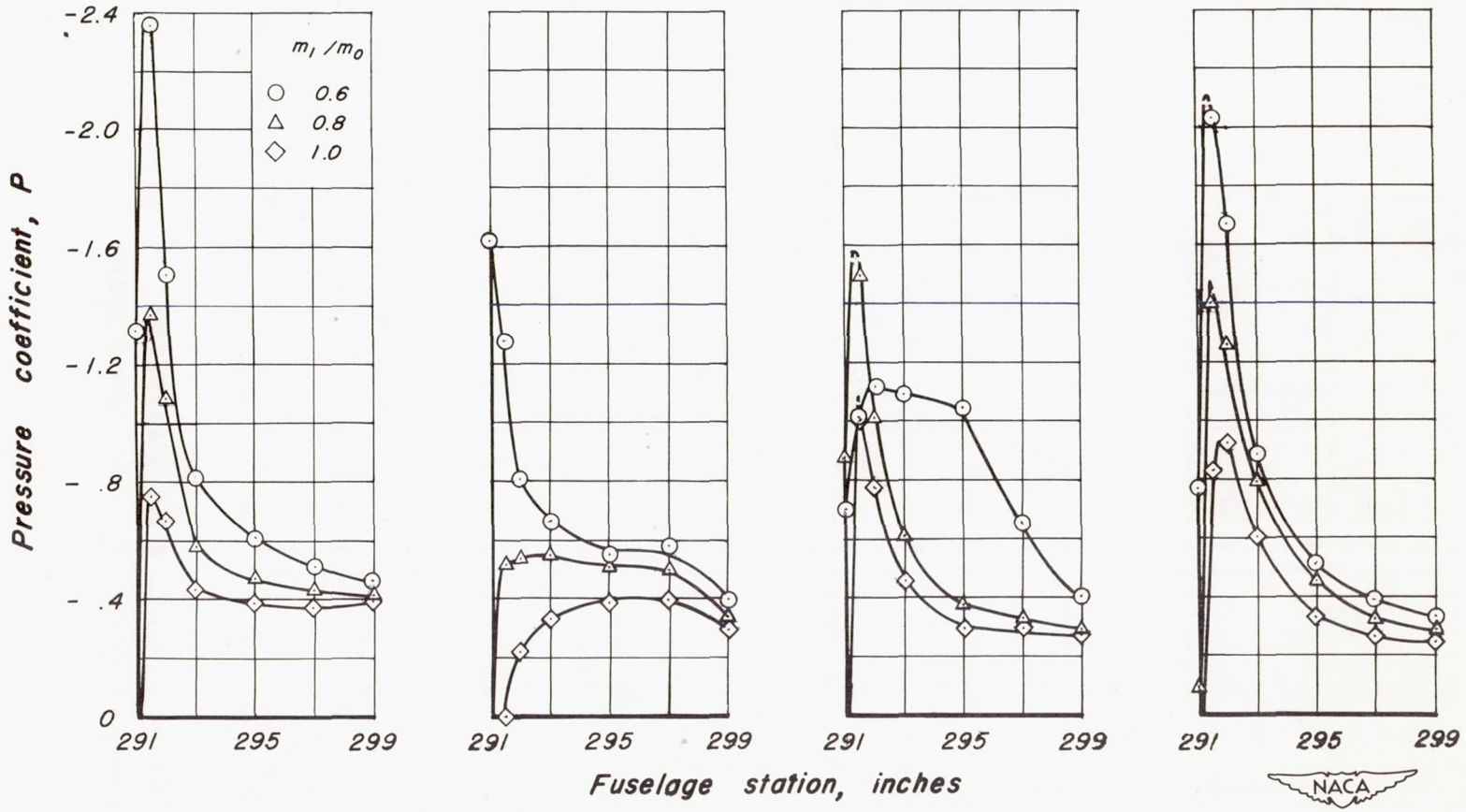

(c) Lip B. (d) Lip D. (e) Lip F. (f) Lip G.

Figure 7.- Concluded.

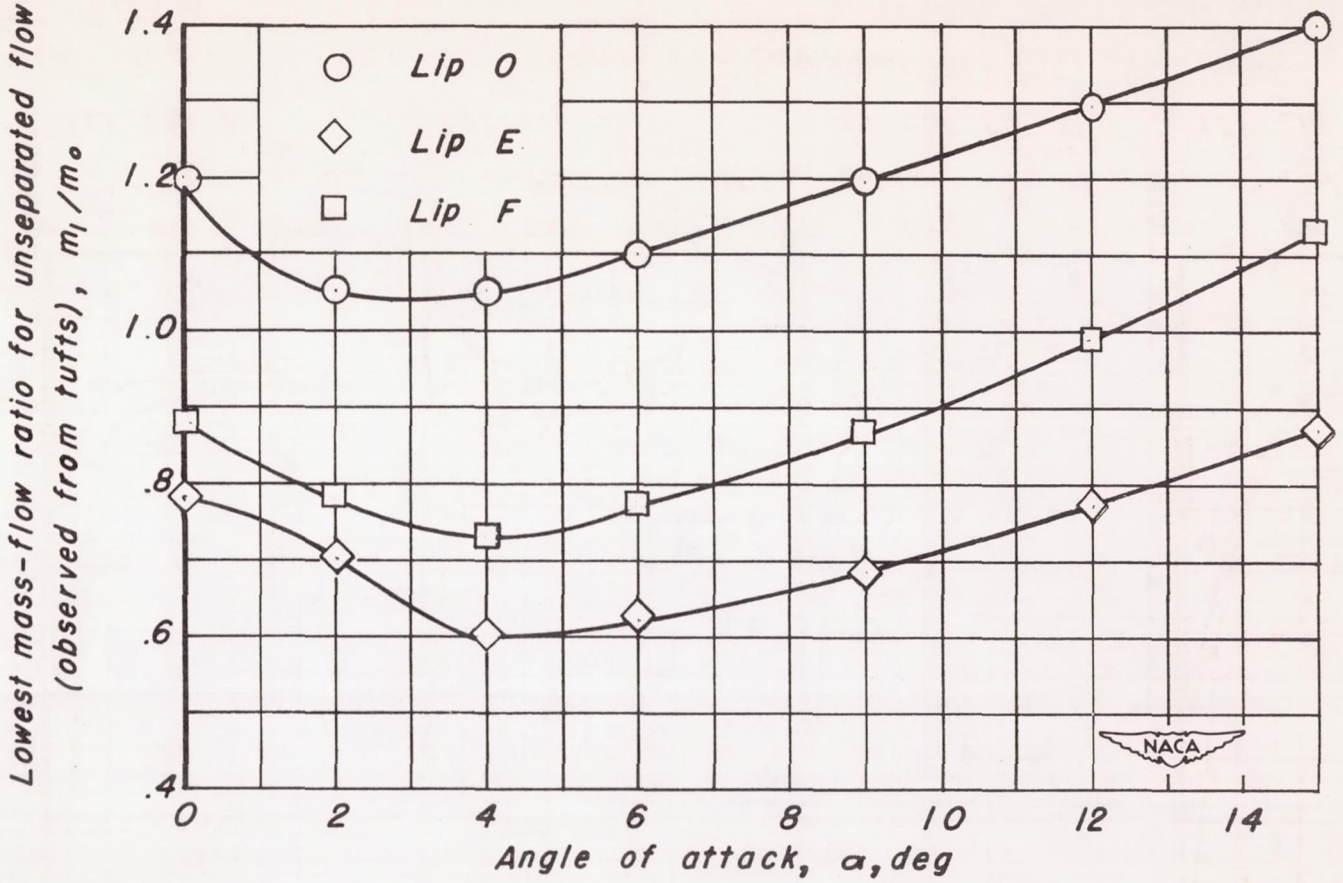

Figure 8.—The variation of the lowest mass-flow ratio for unseparated flow with angle of attack for lips O, E, and F. $\beta = 0°$; $m_B/m_1 = 0.075$.

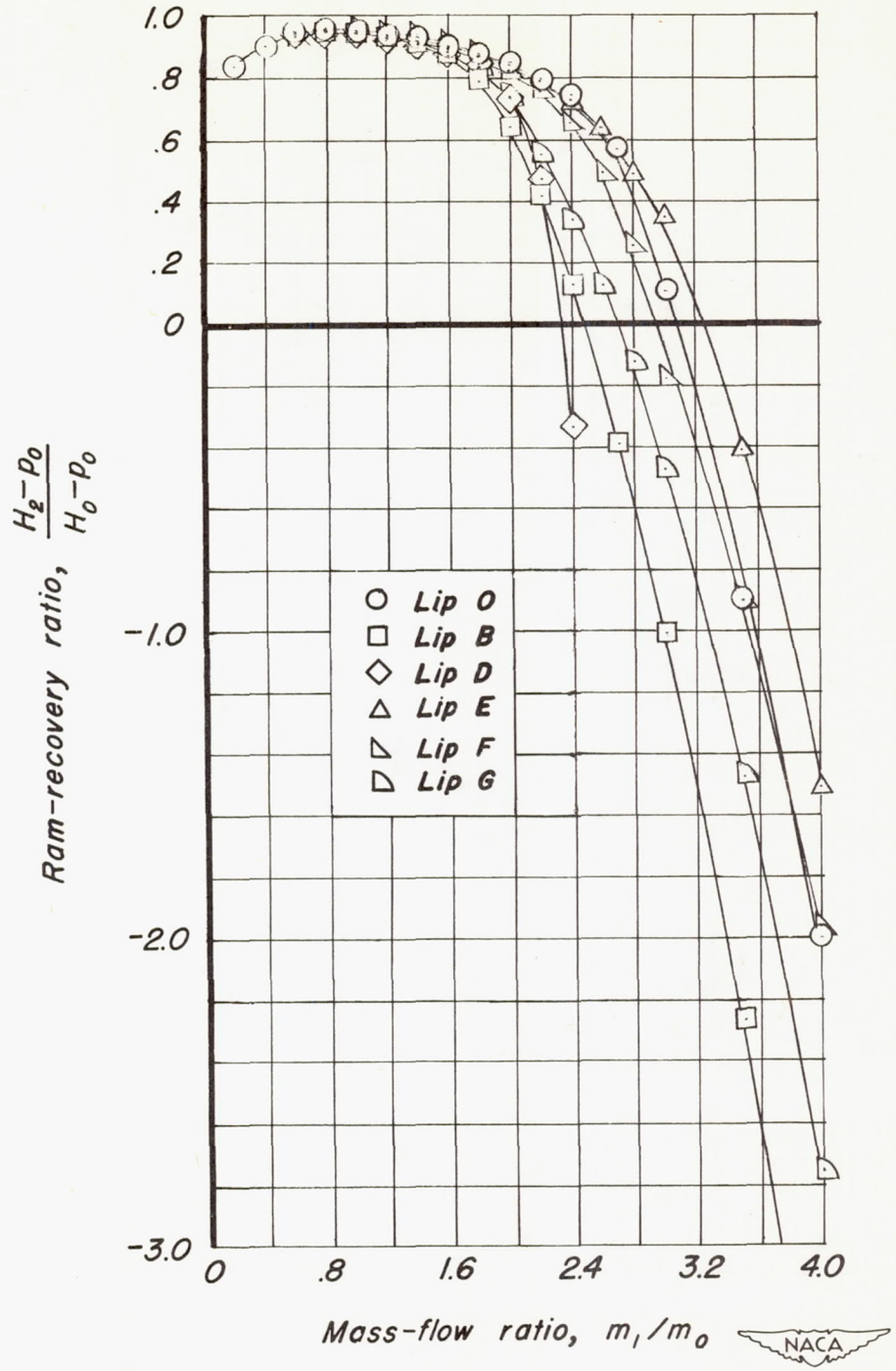

Figure 9.—The variation of the ram-recovery ratio with mass-flow ratio for the main duct. $\alpha = 0°$; $\beta = 0°$; $m_B/m_1 = 0.075$.

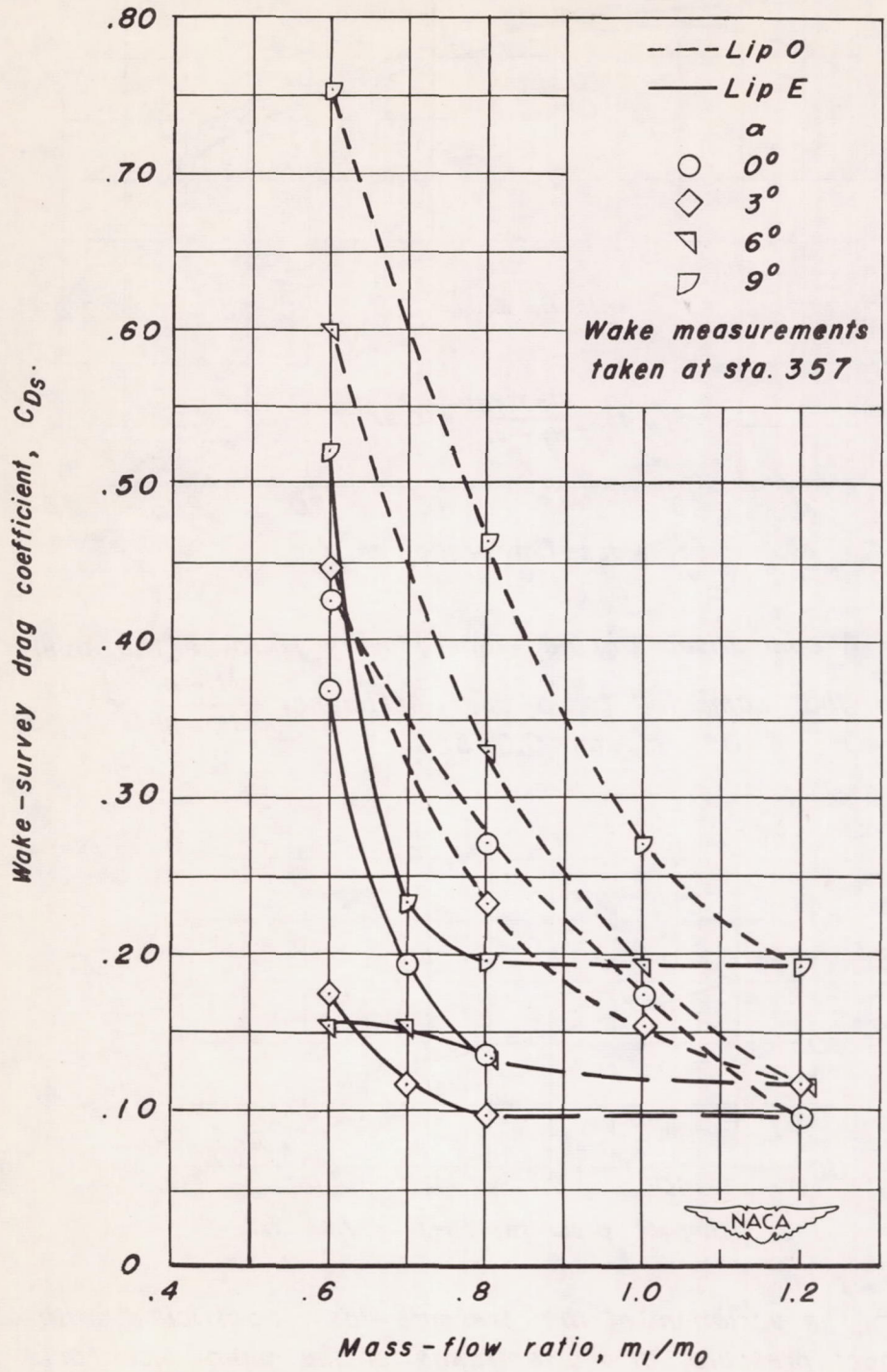

Figure 10.- A comparison of the wake-survey drag coefficients of lip O and lip E for various mass-flow ratios and angles of attack. $\beta = 0°$; $m_B/m_1 = 0.075$.

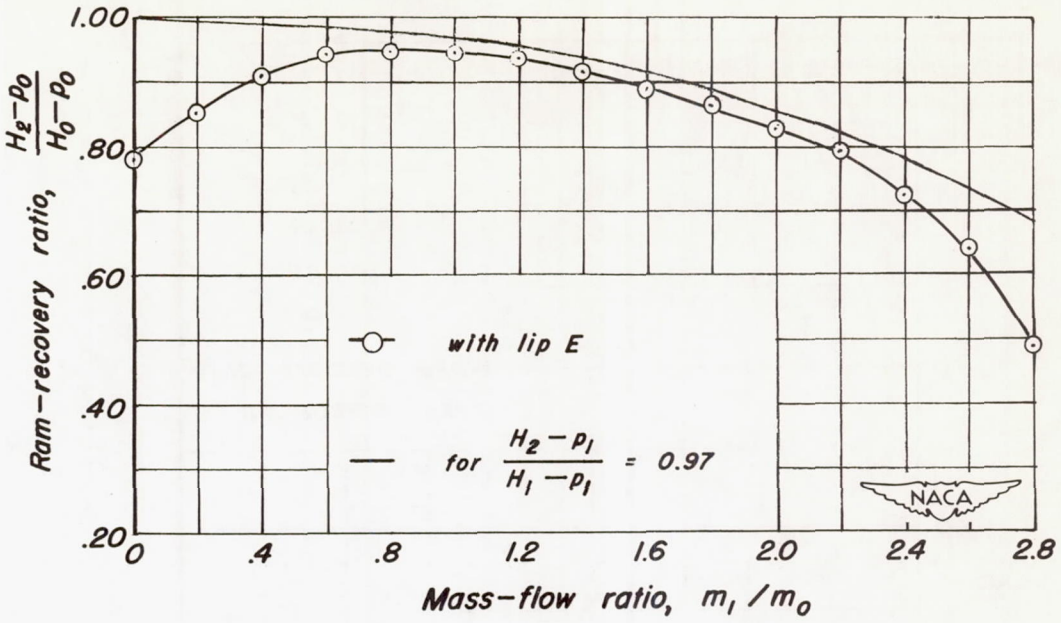

Figure 11.– A comparison of the ram-recovery ratio in the main duct with that computed for a duct efficiency $\frac{H_2-p_1}{H_1-p_1}$ of 0.97. $\alpha=0°$; $\beta=0°$; $m_B/m_1=0.075$.

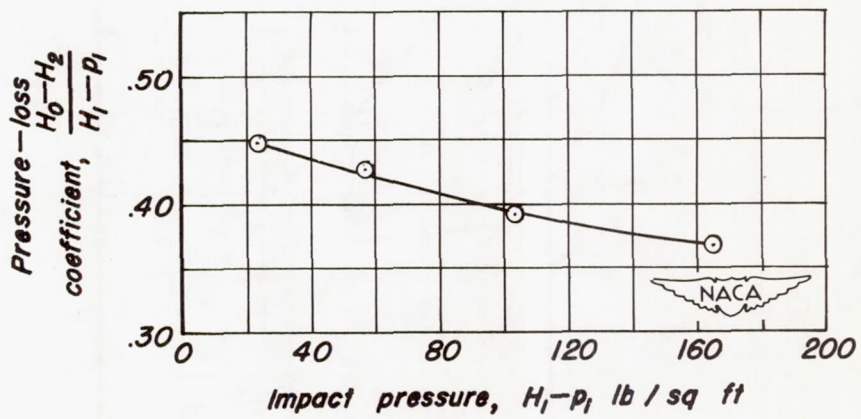

Figure 12.– The variation of the pressure-loss coefficient with the impact pressure at the entrance of the main duct for a simulated power-on static condition. $\alpha=0°$; $\beta=0°$; $m_B/m_1=0.075$.

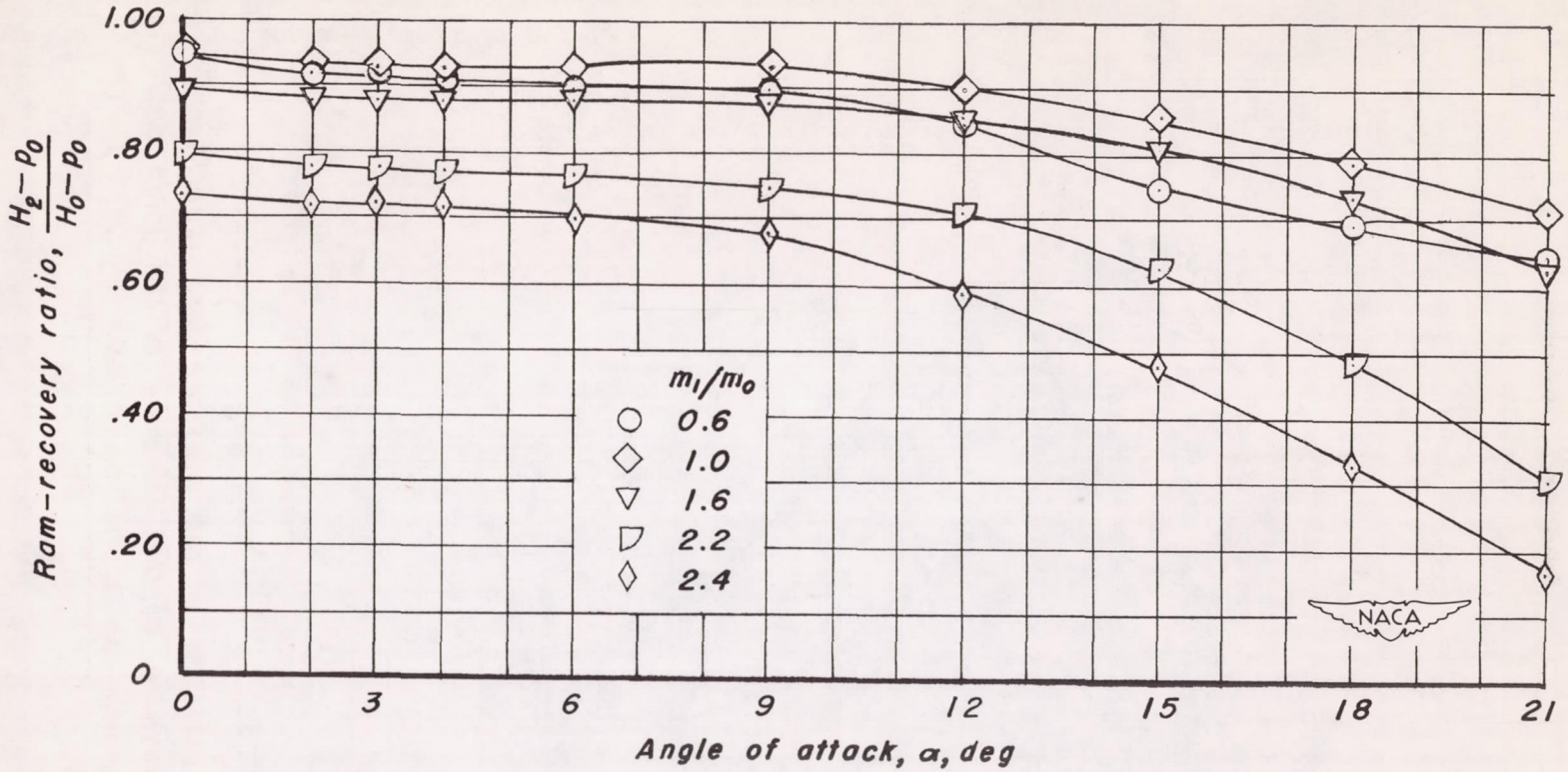

Figure 13.– The variation of the ram-recovery ratio in the main duct with angle of attack for various mass-flow ratios. $\beta = 0°$; $m_B/m_1 = 0.075$.

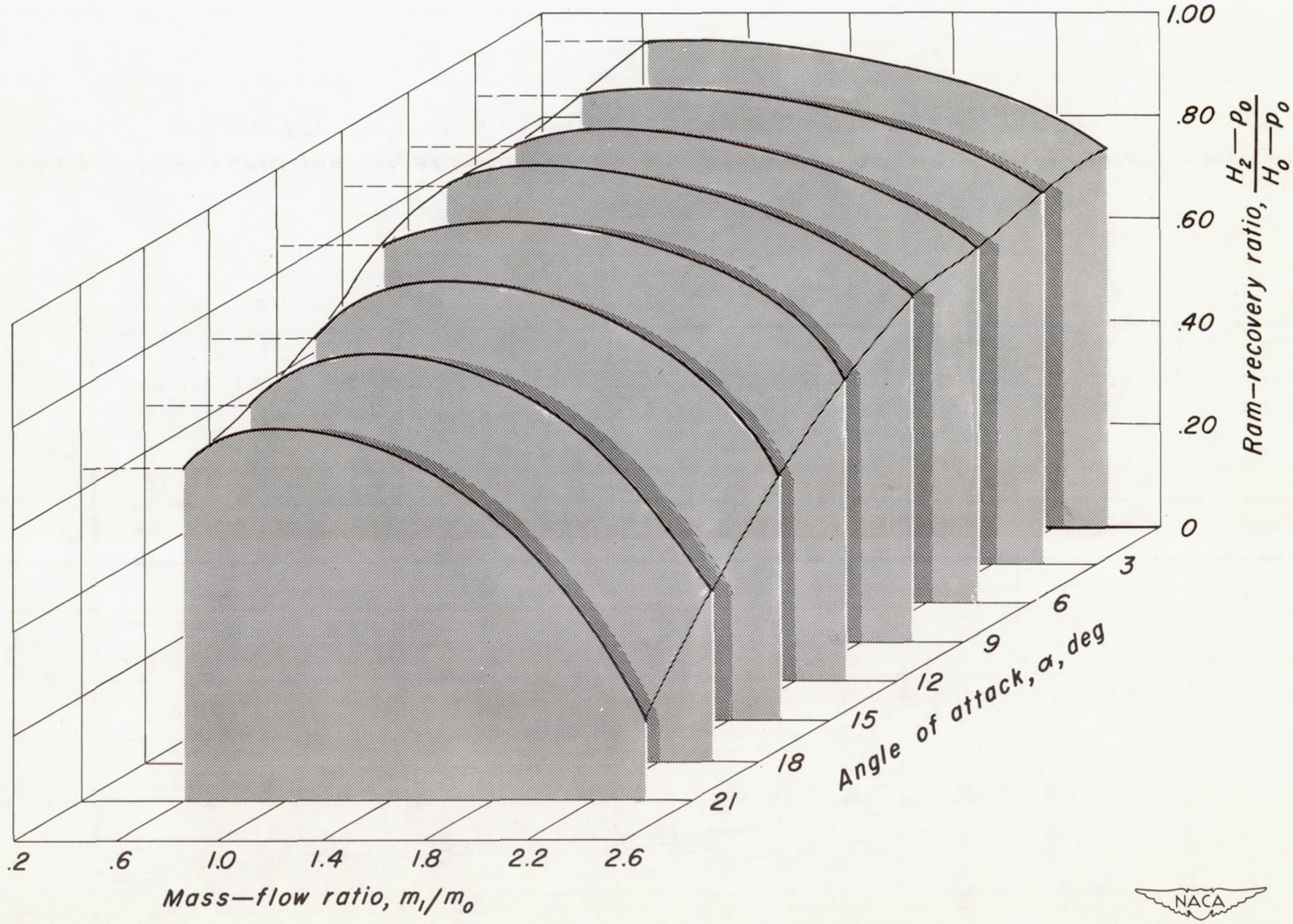

Figure 14.—The variation of the ram-recovery ratio in the main duct with mass-flow ratio and angle of attack. $\beta = 0°$; $m_B/m_1 = 0.075$.

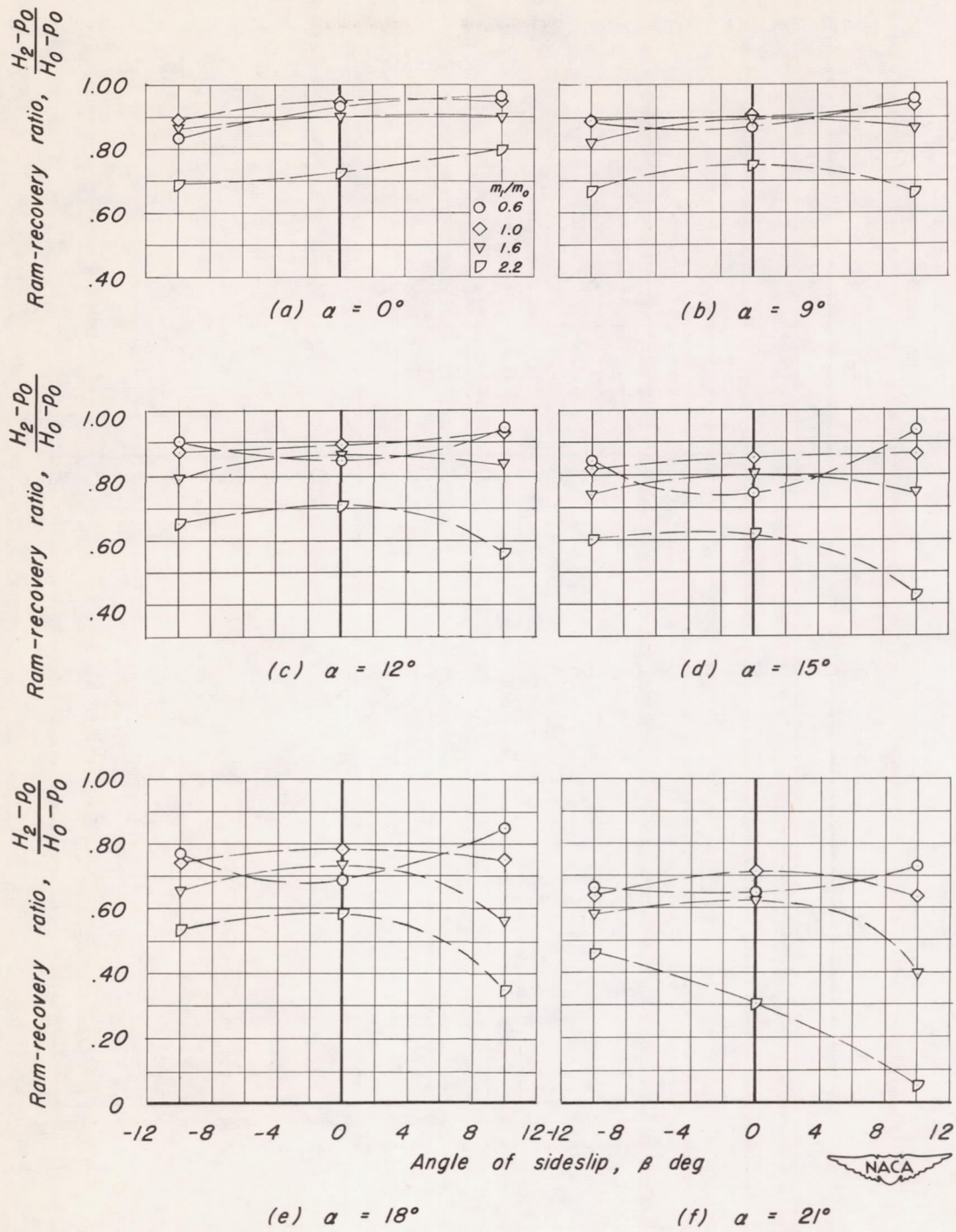

Figure 15.—The effect of angle of sideslip on the ram-recovery ratio in the main duct for various mass-flow ratios. $m_B/m_1 = 0.075$.

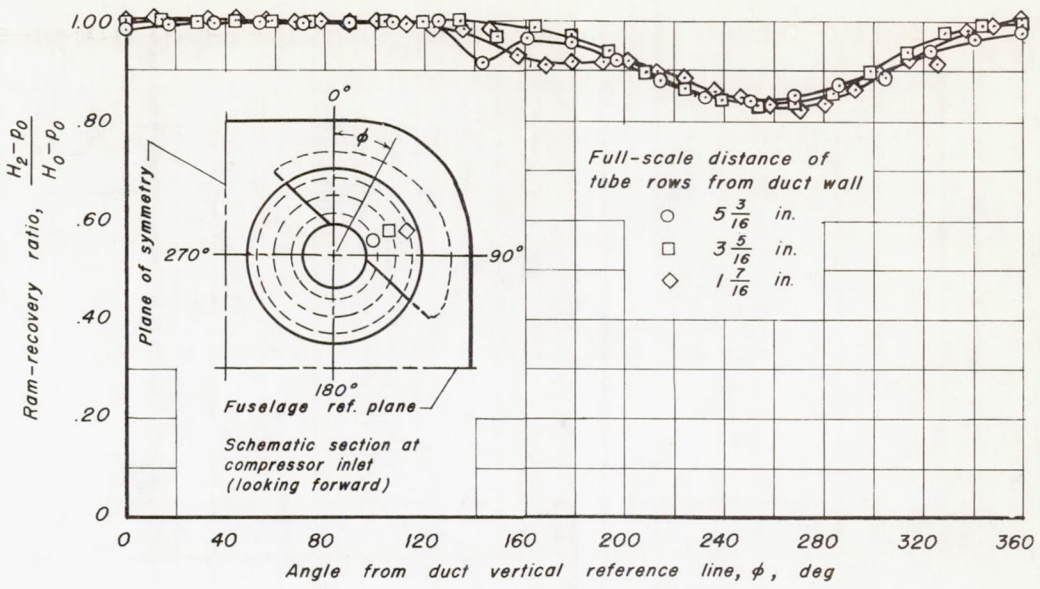

(a) $m_1/m_0 = 0.6$

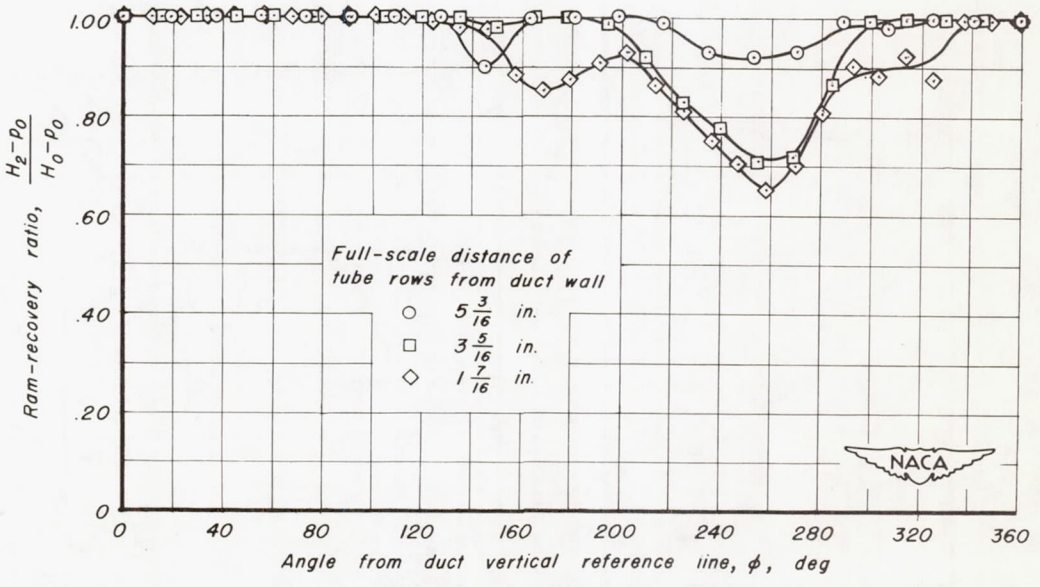

(b) $m_1/m_0 = 0.8$

Figure 16.—The circumferential variation of the ram-recovery ratio at the compressor inlet station. $\alpha = 0°$; $\beta = 0°$; $m_B/m_1 = 0.075$.

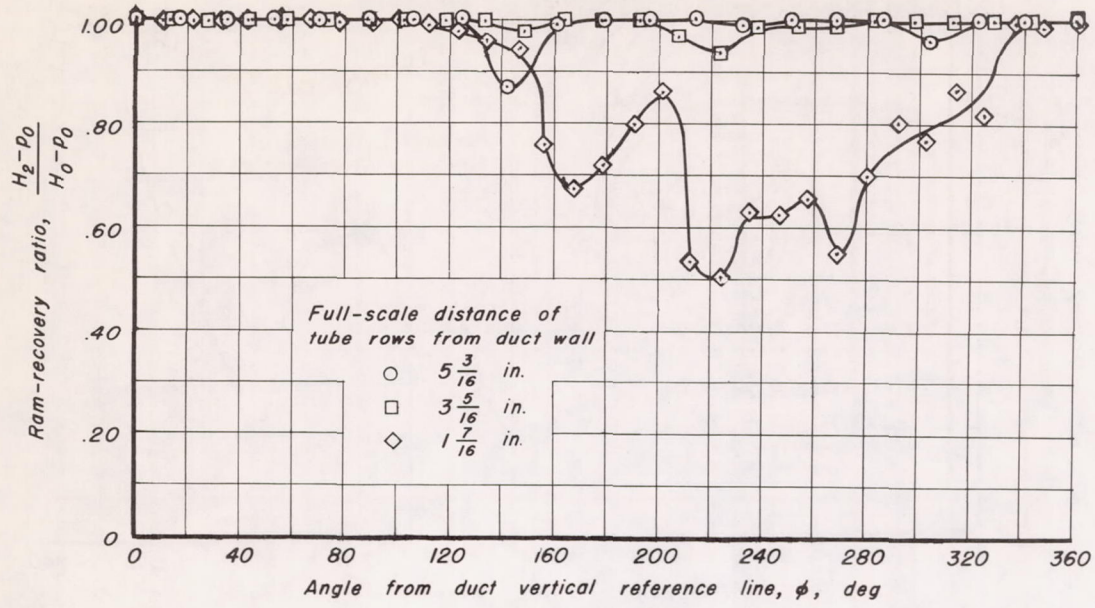

(c) $m_1/m_0 = 1.2$

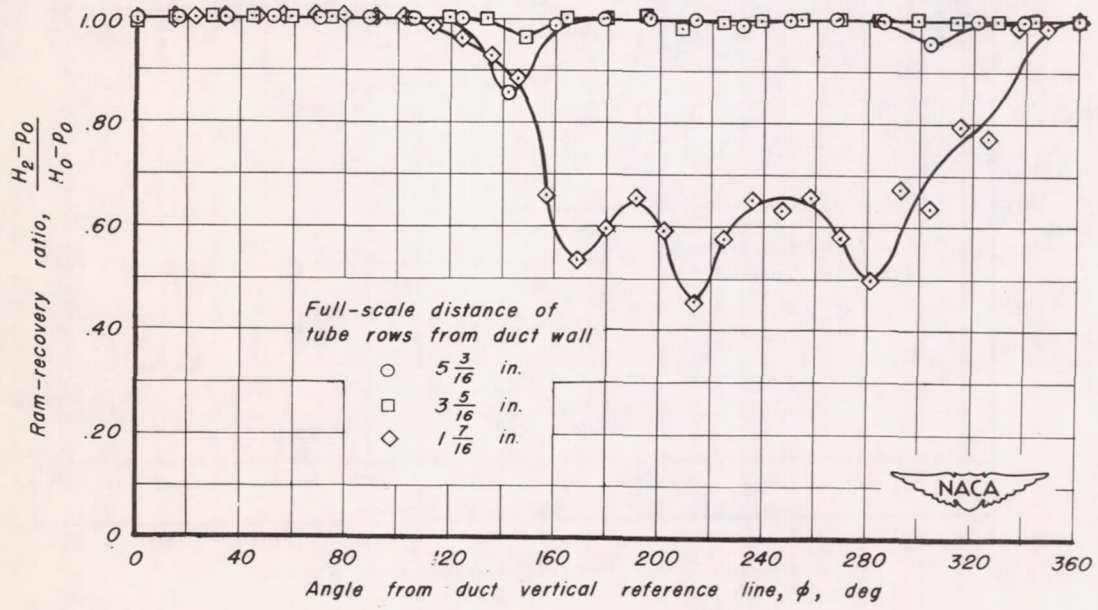

(d) $m_1/m_0 = 1.4$.

Figure 16.- Continued.

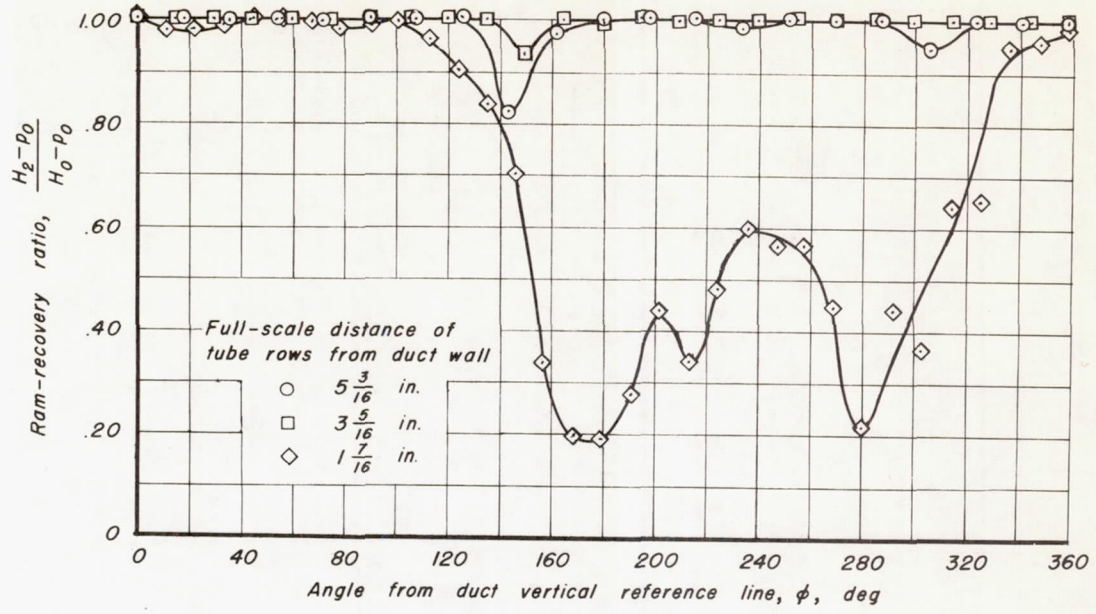

(e) $m_1/m_0 = 1.8$

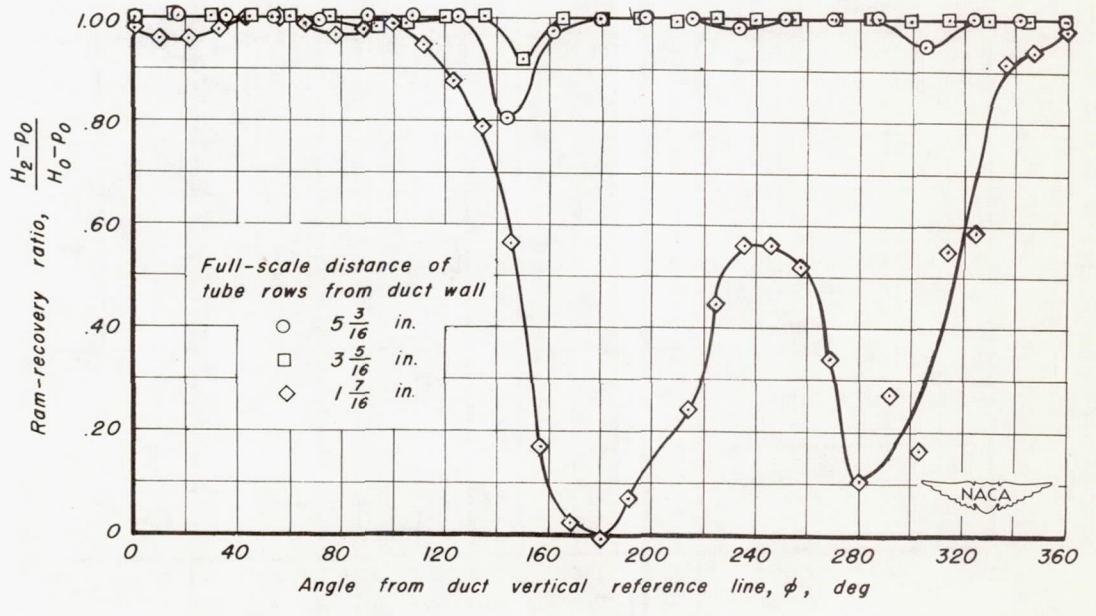

(f) $m_1/m_0 = 2.0$.

Figure 16.- Concluded.

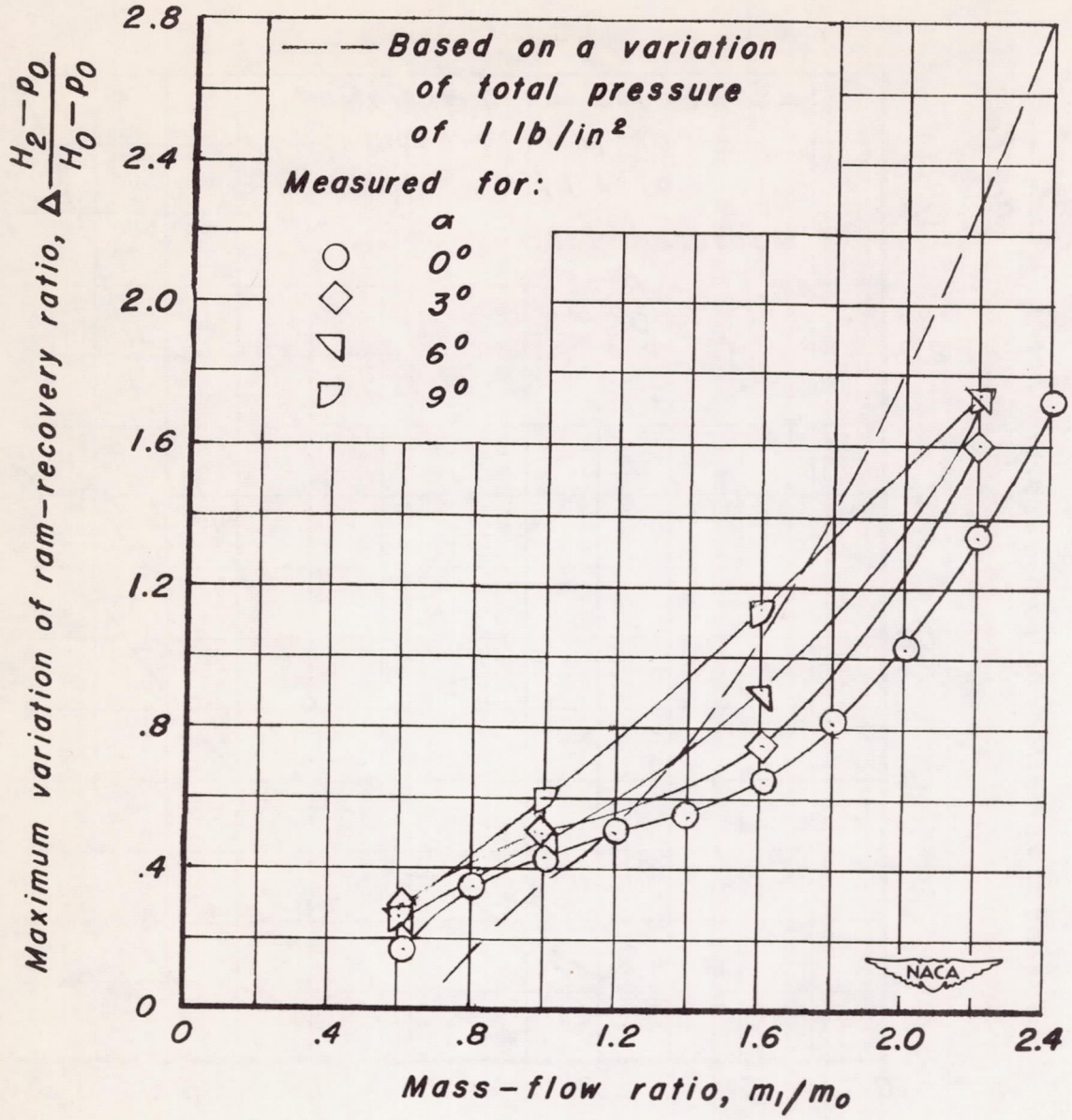

(a) Effect of angle of attack. $\beta = 0°$

Figure 17.– The maximum circumferential variation of ram-recovery ratio in the main duct for various mass-flow ratios. $m_B/m_1 = 0.075$.

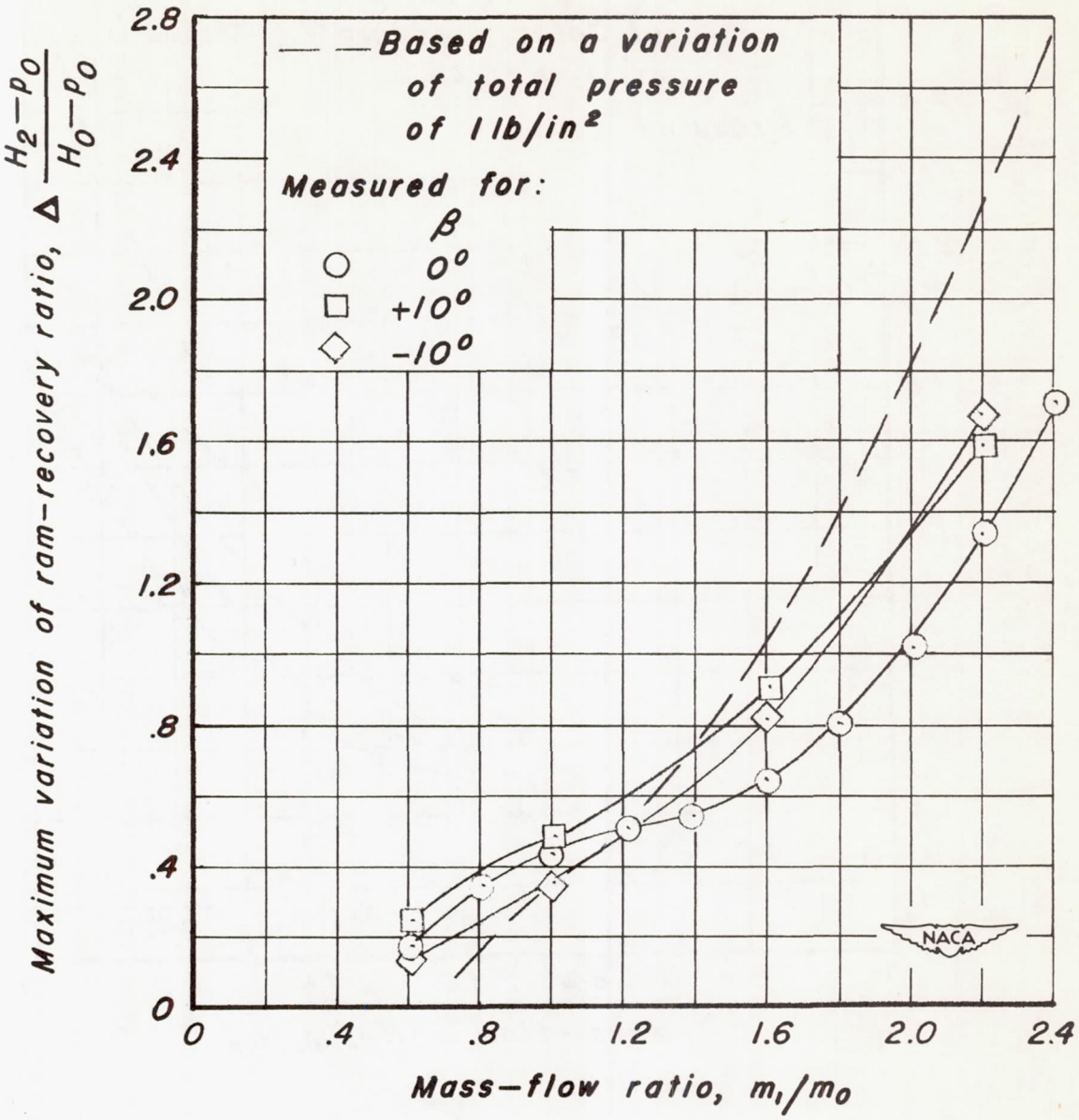

(b) Effect of angle of sideslip. $\alpha = 0°$

Figure 17.— Concluded.

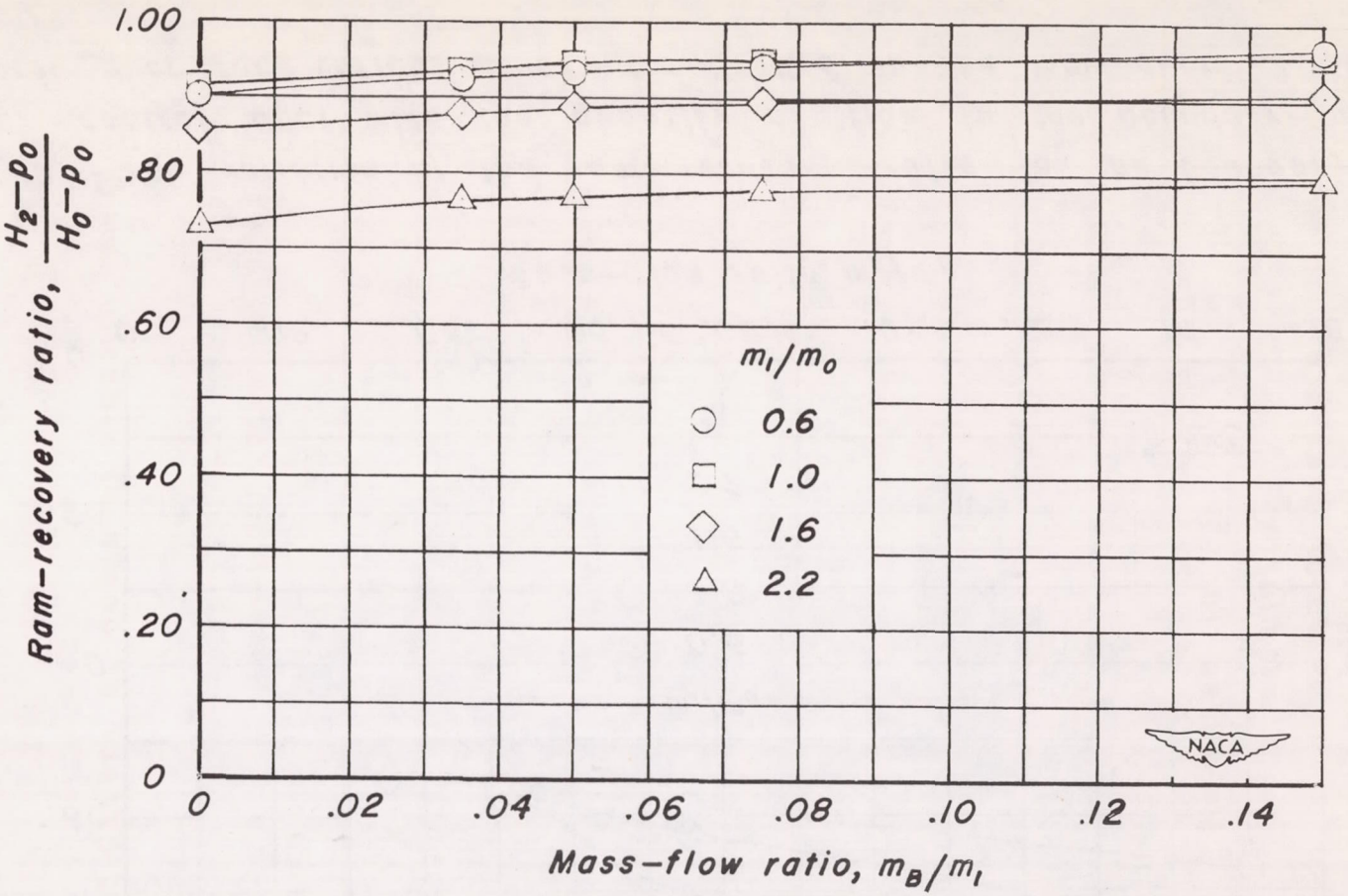

Figure 18.—The effect of the quantity of flow in the boundary-layer-control duct on the ram-recovery ratio in the main duct for various mass-flow ratios. $\alpha = 0°$; $\beta = 0°$.

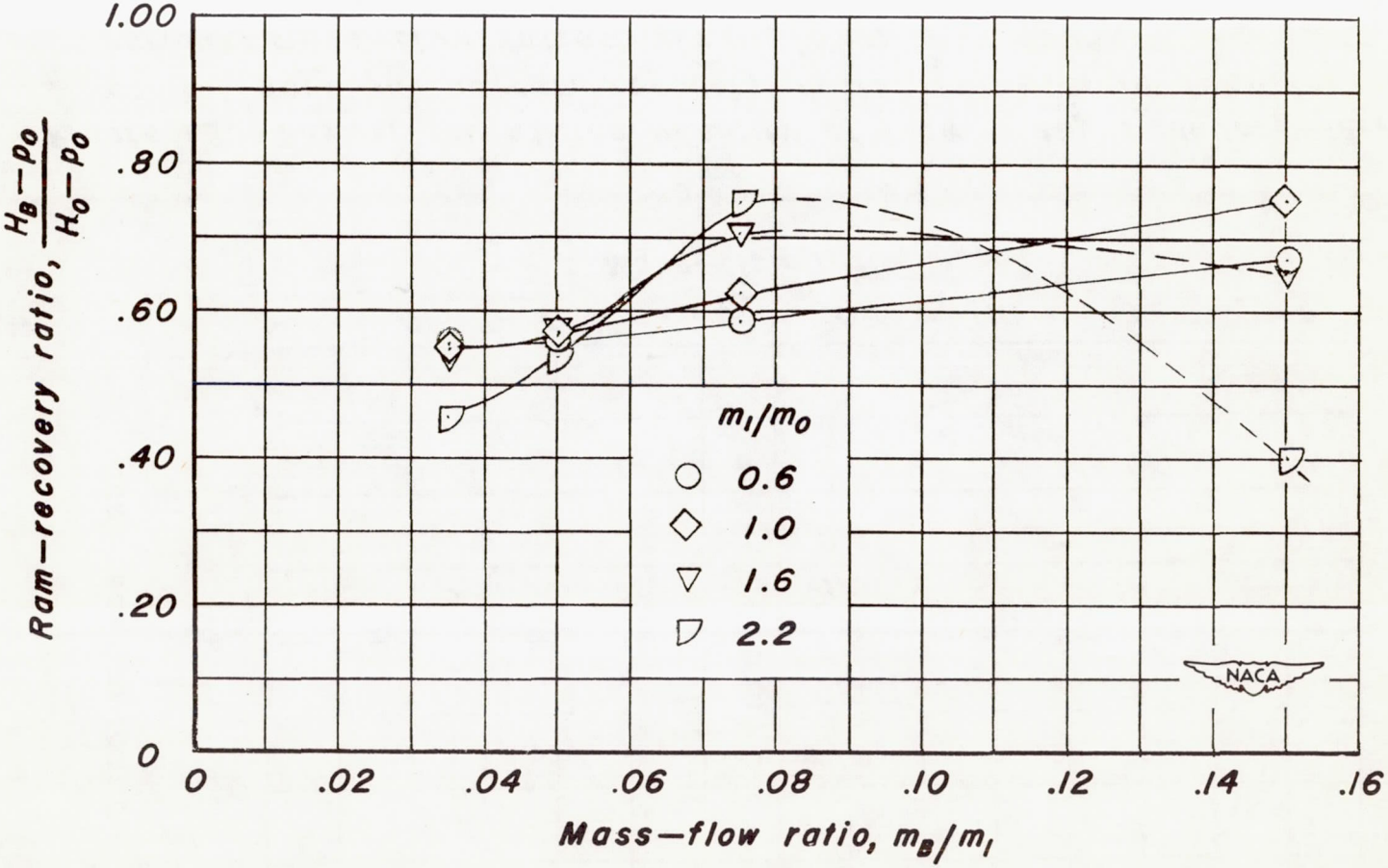

Figure 19.— The variation of the ram-recovery ratio in the boundary-layer-control duct with the quantity of flow in the boundary-layer-control duct for various mass-flow ratios in the main duct. $\alpha = 0°$; $\beta = 0°$.

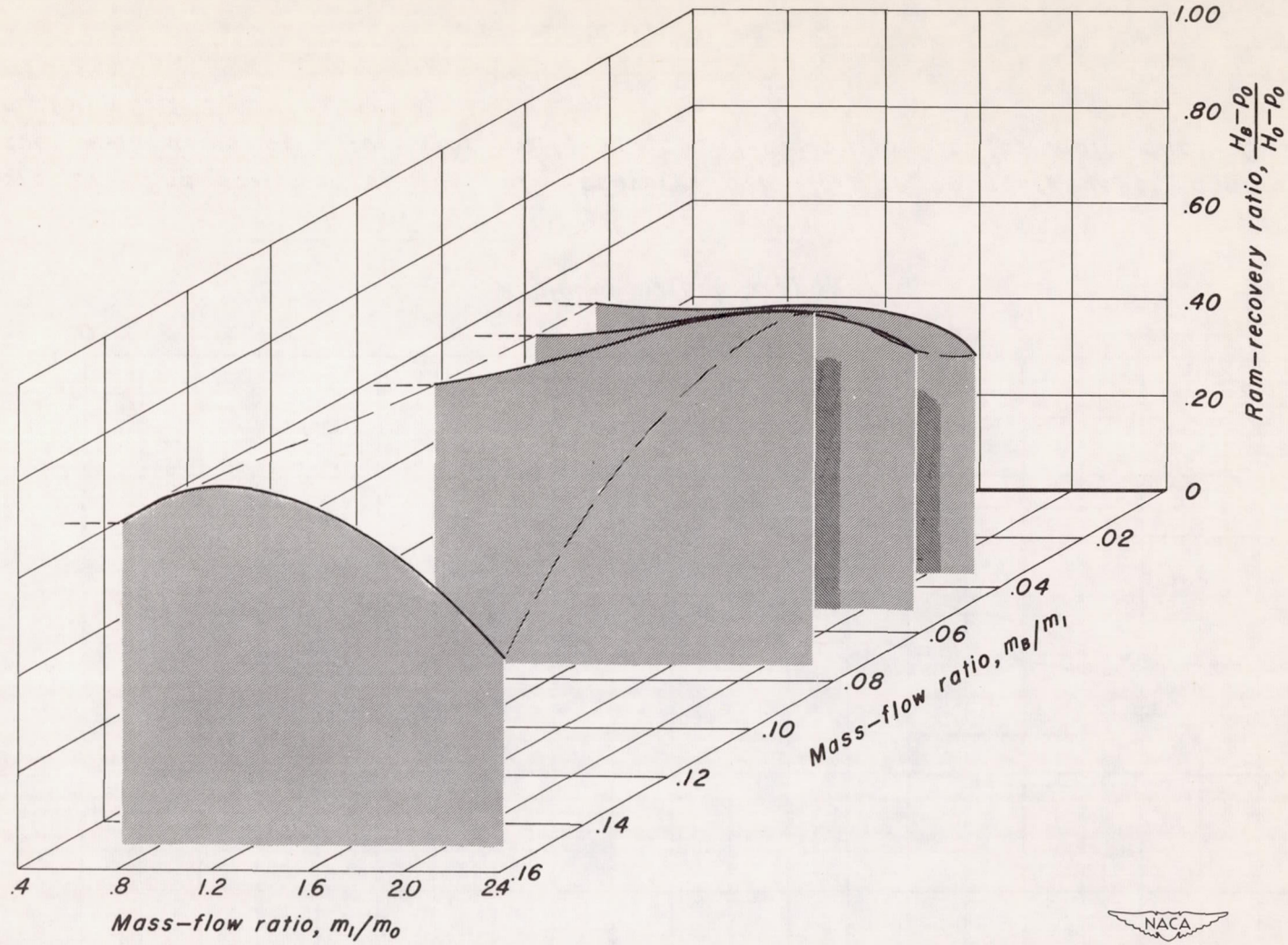

Figure 20.—The variation of the ram-recovery ratio in the boundary-layer-control duct with the mass-flow ratios of the main and boundary-layer-control ducts. $\alpha = 0°$; $\beta = 0°$.

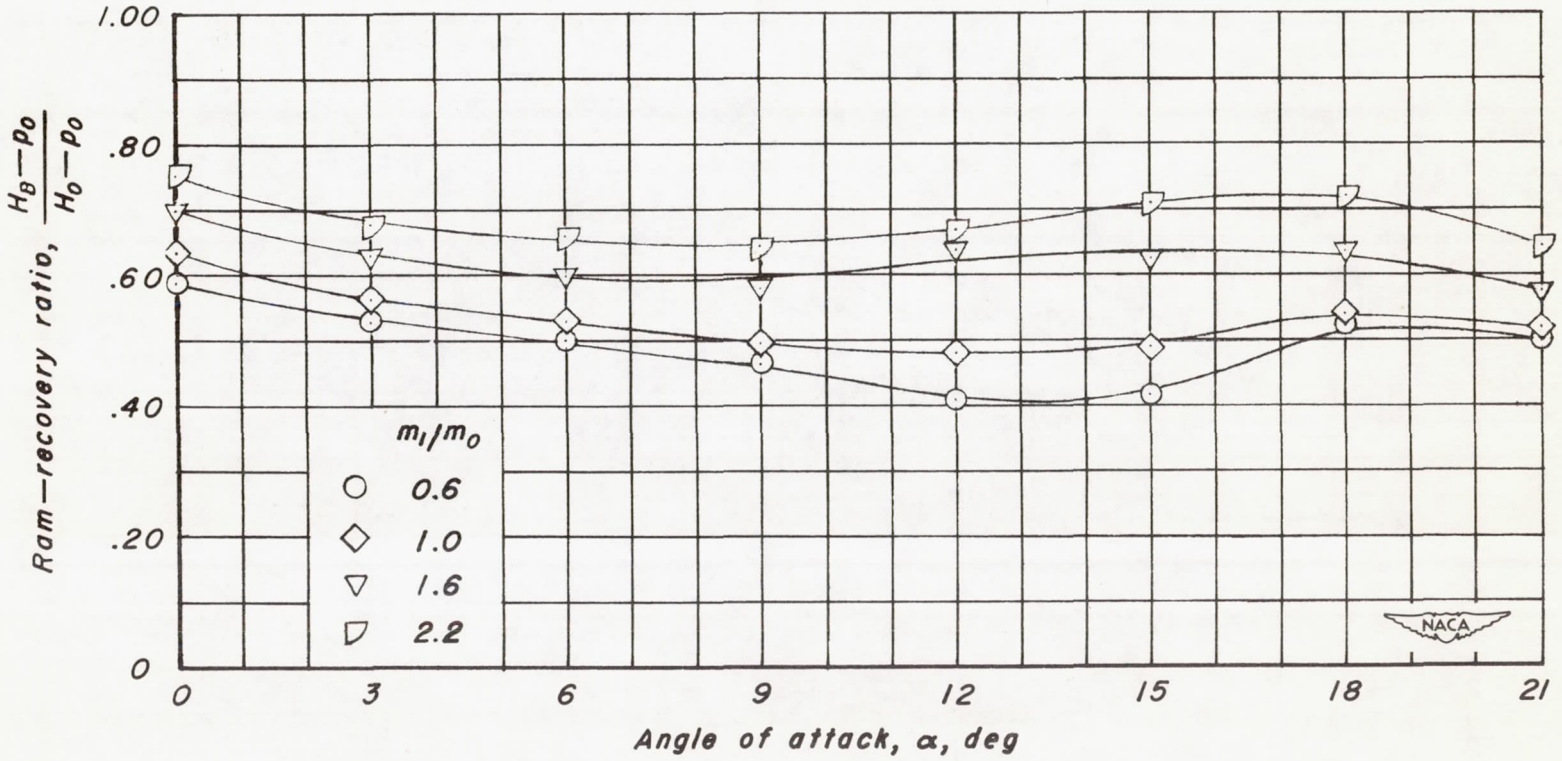

Figure 21.— The variation of the ram-recovery ratio in the boundary-layer-control duct with angle of attack for various mass-flow ratios in the main duct. $\beta = 0°$; $m_B/m_1 = 0.075$.

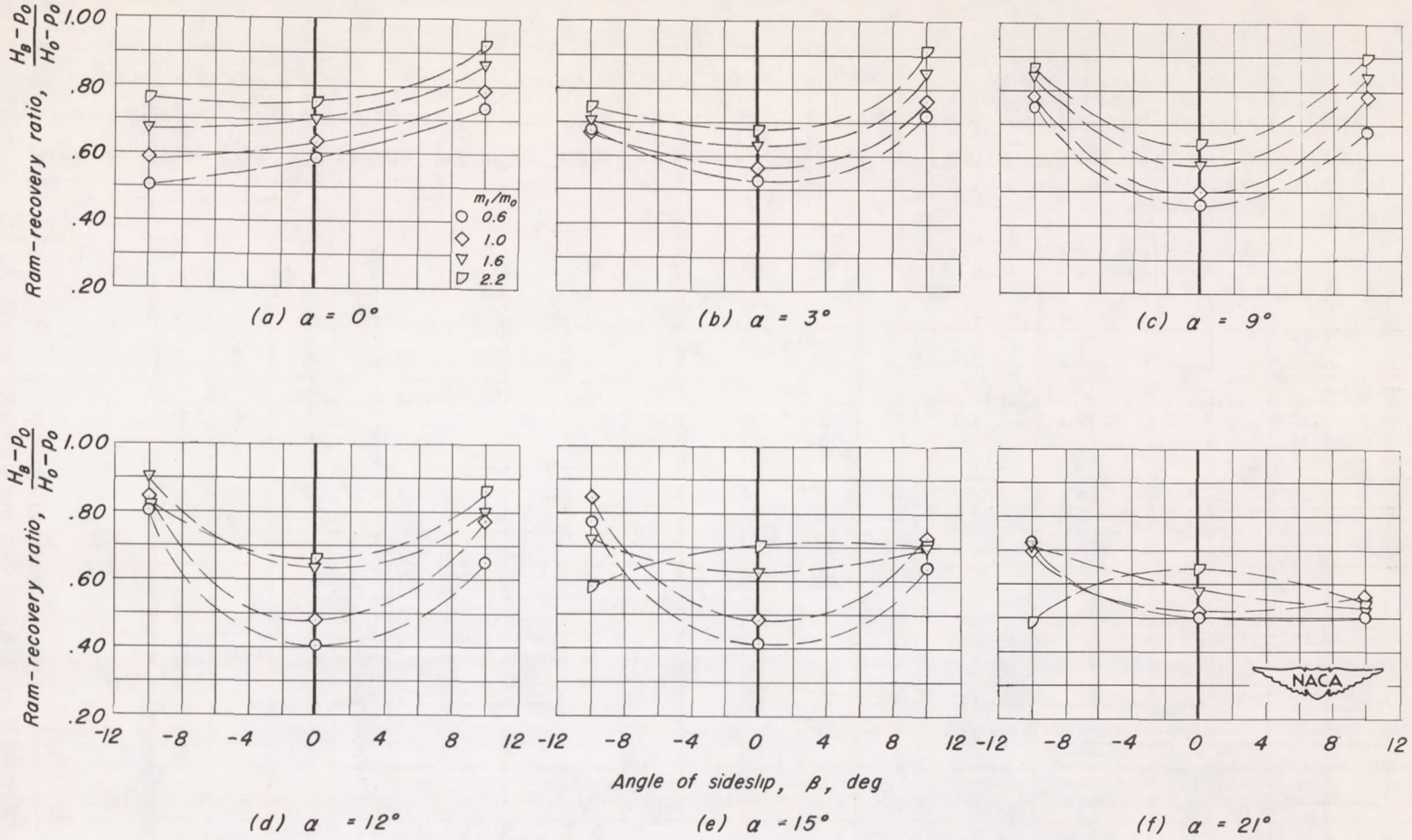

Figure 22.—The effect of angle of sideslip on the ram-recovery ratio in the boundary-layer-control duct for various mass-flow ratios in the main duct. $m_B/m_1 = 0.075$.

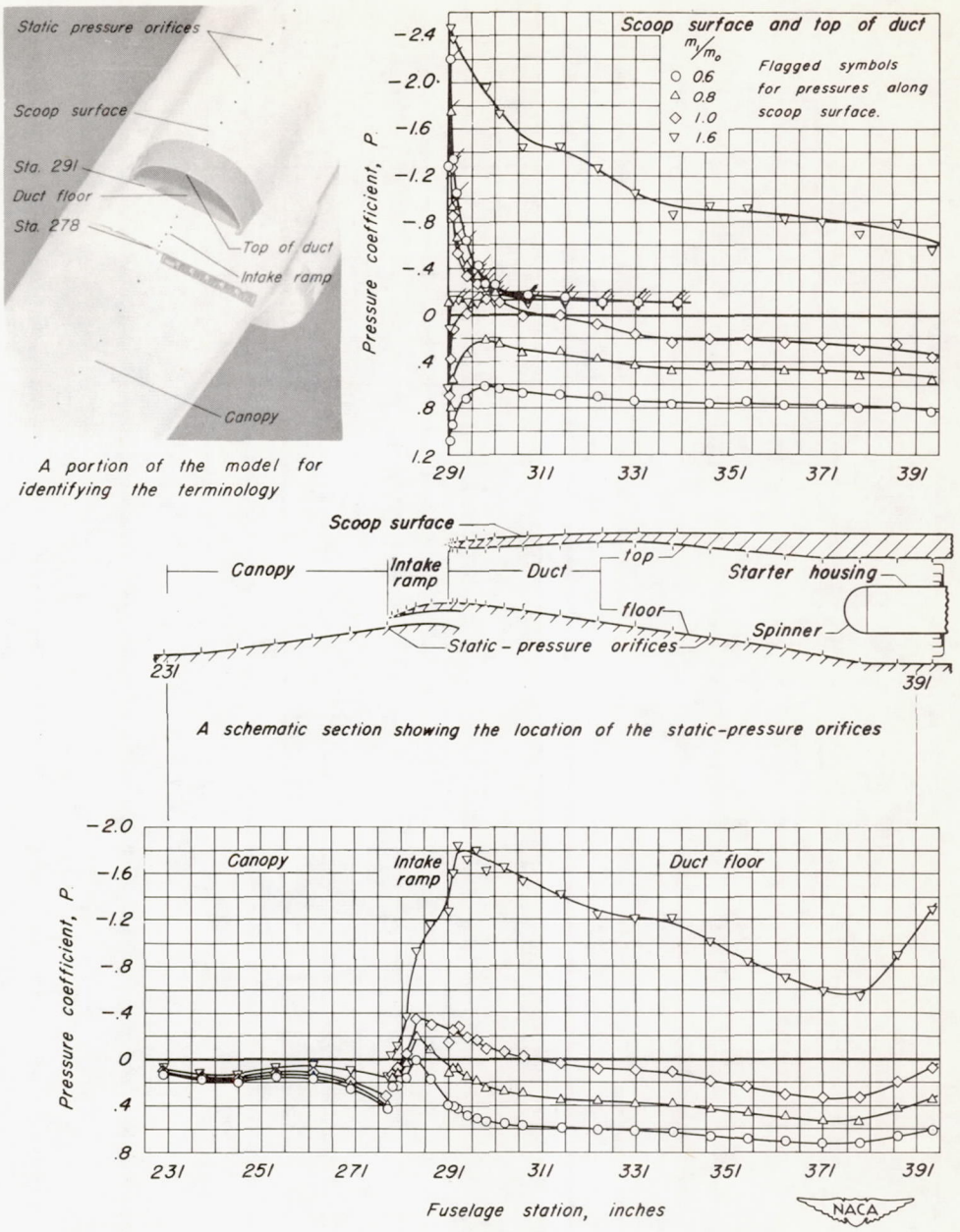

Figure 23.- Pressure coefficients for the canopy, intake ramp, scoop surface, and main duct for various mass-flow ratios. $\alpha = 0°$; $\beta = 0°$; $m_B/m_j = 0.075$.

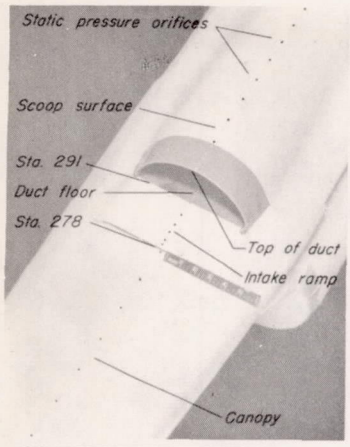

A portion of the model for identifying the terminology

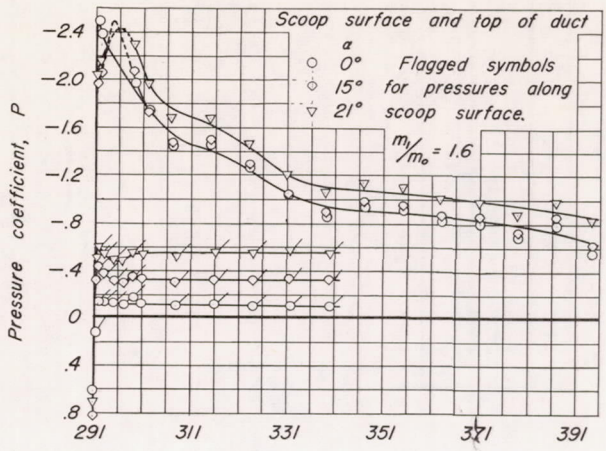

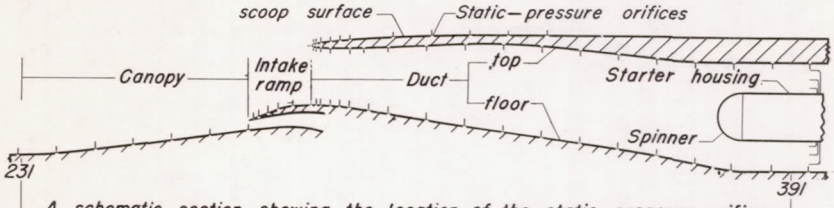

A schematic section showing the location of the static-pressure orifices

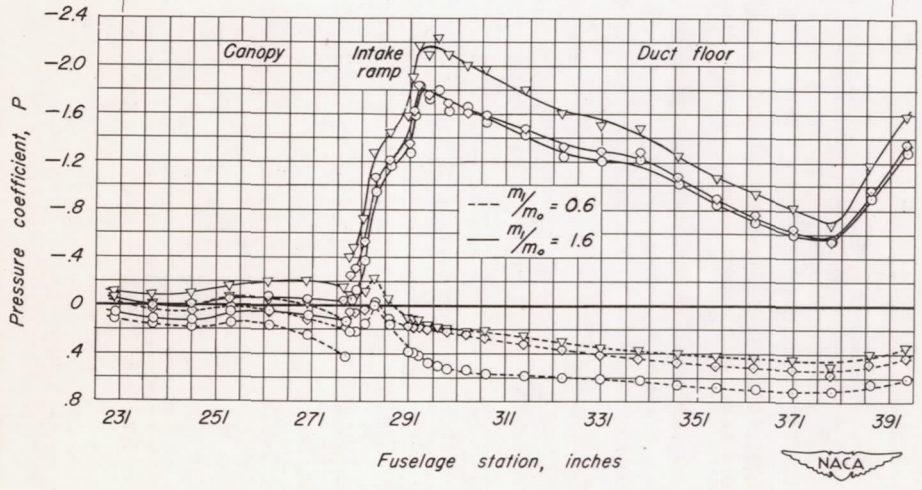

Figure 24.- The effect of angle of attack on the pressure coefficients for the canopy, intake ramp, scoop surface, and main duct. $\beta = 0°$; $m_B/m_l = 0.075$.

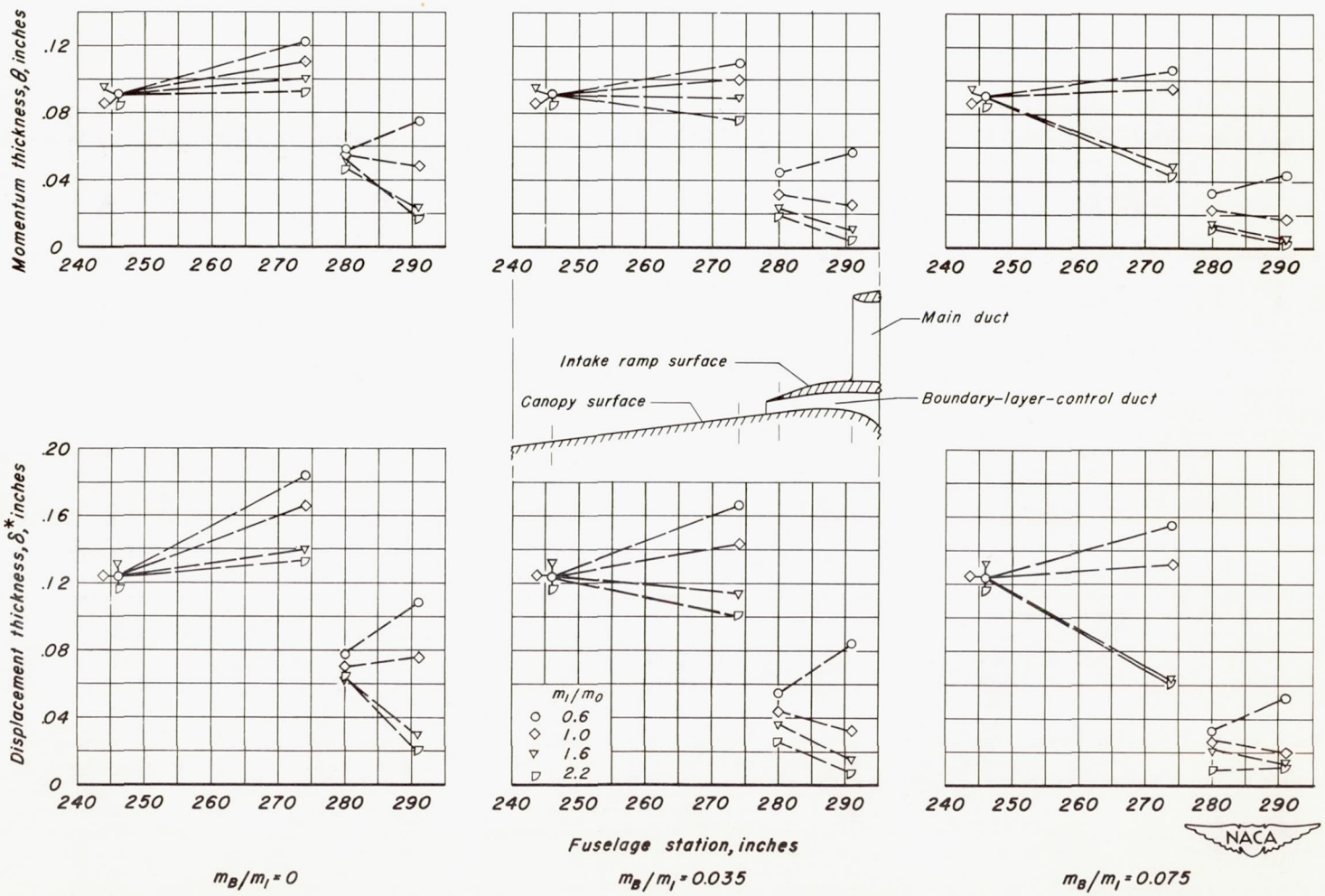

Figure 25.– The momentum and displacement thicknesses of the boundary layer on the canopy and intake ramp for various flow conditions in the main and boundary-layer-control ducts. $\alpha = 0°$; $\beta = 0°$.